MCR-CO_2 global monthly anthropogenic CO_2 emissions at 0.05° for 1970–2025

Franz Pablo Antezana Lopez[1,2*], Guanhua Zhou[1*], Alejandro Casallas[3,4], Kai Zhang[5], Aamir Ali[2], Hongzhi Jiang[1], Jose Luis Alanoca Limachi[2]

[1] School of Instrumentation Science and Optoelectronic Engineering, Beihang University, Beijing 100191, China.

[2] Hangzhou International Innovation Institute, Beihang University, Hangzhou, China.

[3] Institute of Science and Technology Austria, Klosterneuburg 3400, Austria.

[4] Atmospheric Chemistry Department, Max Planck Institute for Chemistry, 55128 Mainz, Germany.

[5] State Key Laboratory of Environmental Criteria and Risk Assessment, Chinese Research Academy of Environmental Sciences, Beijing 100012, China.

Correspondence to: Guanhua Zhou (zhouguanhua@buaa.edu.cn)

Abstract. Long-term anthropogenic carbon dioxide (CO_2) inventories support atmospheric modelling and historical emission assessment, but rarely combine monthly continuity, fine spatial detail and consistent sector definitions. We present the Multisource Constraint-based Reconstruction of CO_2 emissions (MCR-CO_2), a global monthly inventory at 0.05° resolution for January 1970–December 2025. The record comprises 672 months and seven terrestrial sectors. MCR-CO_2 combines compatible annual and monthly inventories with sector-specific geographical information. Annual country–sector budgets, monthly fractions and fine-grid allocation are reconstructed separately under explicit mass-conservation constraints. Terrestrial emissions increase from 15.140 Gt CO_2 in 1970 to 39.075 Gt in 2024 and 39.385 Gt in 2025. Including aviation and shipping gives 41.380 Gt CO_2 in 2025. Historical source-withholding tests identify sector-dependent benefits from monthly information. Against CAMS-REG in Europe, spatial Jensen–Shannon similarity increases from 46.2% for EDGAR to 48.0% for MCR-CO_2, while normalised RMSE decreases from 10.976 to 8.957. Against Vulcan V4 in the United States, similarity increases from 37.6% to 47.8%, while normalised RMSE decreases from 10.345 to 9.942. Comparisons with ODIAC, 400 alternative source configurations and predictor-removal experiments assess sensitivity to the available inputs. A separate 1,000-member Monte Carlo experiment propagates EDGAR-referenced annual-budget uncertainty through the normalised monthly and spatial allocation, conditional on fixed reconstruction weights. Together, these assessments make the record useful for analysing long-term emission geography and seasonality with traceable accounting and uncertainty assumptions. The dataset is available at https://doi.org/10.5281/zenodo.23337181 (Antezana Lopez, 2026a).

1 Introduction

Spatially and temporally resolved anthropogenic carbon dioxide (CO_2) inventories are essential for atmospheric transport studies, emission assessments and analyses of historical energy use. These applications require seasonal and geographical information that global annual totals alone cannot provide. Historical activity estimates are generally more complete at national and annual scales than at monthly and fine-grid scales. Modern spatial observations also cannot establish where emitters operated in earlier decades (Oda et al., 2018; Crippa et al., 2024).

Established inventories provide complementary parts of this record. EDGAR supplies long-term country–sector estimates and gridded products (Crippa et al., 2024), while CEDS provides historical sectoral trajectories (Hoesly et al., 2018). Li et al. (2026) add daily emission estimates for selected countries and activities. MEIC includes distinct China and global products with detailed source categories (Zheng et al., 2018; Xu et al., 2024). ODIAC resolves fine-scale fossil-fuel emission patterns (Oda et al., 2018). These products differ in temporal coverage, resolution and accounting boundaries. MCR-CO_2 connects their compatible information in a single 1970–2025 monthly record at 0.05° with seven terrestrial sectors.

MCR-CO_2 separates emission magnitude, seasonal timing and geographical placement. The framework first determines compatible annual country–sector budgets, reconstructs their monthly distribution, and allocates each monthly amount to eligible 0.05° cells. A bounded recurrent adjustment represents additional plausible emitting locations by redistributing existing mass within the same country, sector and month. This separation keeps the annual, temporal and spatial information traceable throughout the reconstruction.

The inventory contains 672 consecutive monthly fields for power generation, industry, terrestrial transport, buildings, fuel production and transformation, agriculture, and waste. Aviation and shipping are separate products and enter combined totals once. Its contribution is the integration of historical depth, monthly sector detail and fine geographical allocation under common accounting rules. The record supports analyses of changing emission geography and provides spatially explicit anthropogenic inputs for atmospheric modelling.

We evaluate the record through complementary temporal, spatial and uncertainty assessments. Historical source-withholding tests compare monthly timing with uniform allocation and transferred seasonal profiles. CAMS-REG and Vulcan V4 provide regional spatial benchmarks in Europe and the United States. ODIAC comparisons extend the assessment to Brazil, southern Africa and Madagascar, and Australia. Source alternatives and fixed-mass spatial tests assess reconstruction sensitivity, while Monte Carlo propagation quantifies a conditional annual-budget uncertainty component (Sects. 4.1–4.6).

2 Data and methods

MCR-CO_2 combines sector harmonisation, annual calibration, monthly reconstruction and fine-grid allocation, followed by conservation checks (Fig. 1). Annual calibration determines emission magnitude, monthly fractions determine timing, and spatial weights determine geographical placement. A separate recurrent adjustment transfers bounded amounts of existing mass to additional eligible locations. Each stage has an explicit conservation domain.

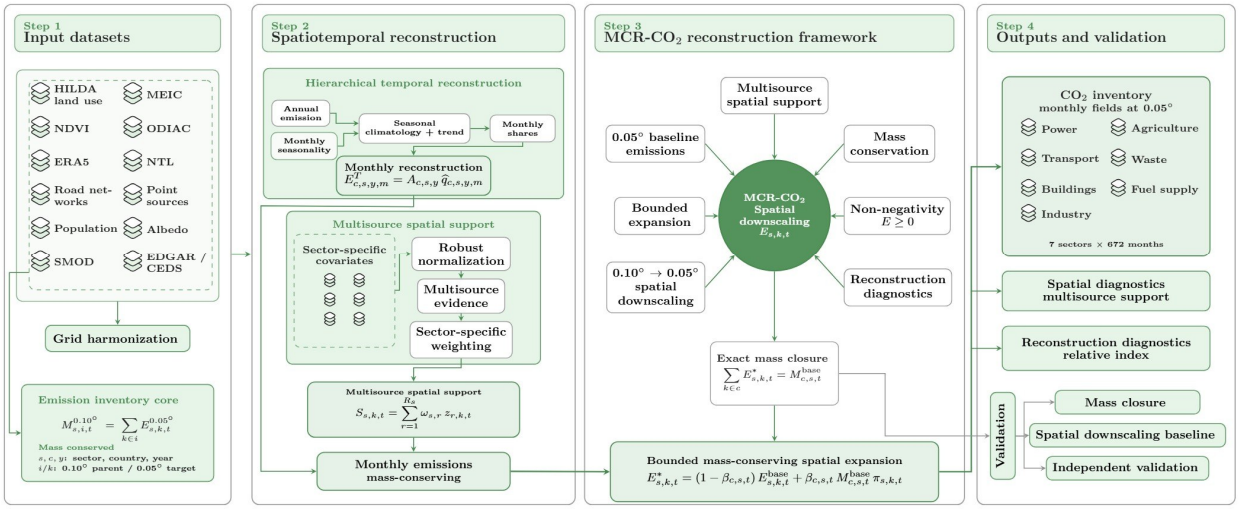


Figure 1. Overview of the MCR-CO_2 reconstruction, from inventory harmonisation and annual calibration to monthly allocation, spatial disaggregation, support adjustment and checks of emission conservation.

2.1 Input data and sector definitions

Input inventories serve complementary roles according to temporal coverage and emitting process. EDGAR supplies annual country–sector estimates and national monthly series for 1970–2024 (European Commission Joint Research Centre, 2025). Its monthly 0.10° sector maps used here cover 2000–2024. CEDS informs long-term annual trajectories, while compatible Li et al. (2026) and MEIC records provide additional subannual information. ODIAC, facility-related grids, roads, settlements, population and night-time lights guide allocation where relevant to the emitting activity. Table 1 and Fig. 2 summarise their coverage and functions.

Table 1. Emission inventories and ancillary datasets used in MCR-CO_2, including temporal coverage, reconstruction roles and access information.

Dataset or variable	Role and provider	Official access or download URL
EDGAR_2025_GHG (annual fossil CO_2)	Annual country/sector totals and 0.10° maps, 1970–2024. CO_2bio separately published; distinguishes fossil from biogenic scope.	https://edgar.jrc.ec.europa.eu/dataset_ghg2025
EDGAR_2025_GHG (monthly fossil CO_2)	Country–sector monthly series 1970–2024; sectoral monthly 0.10° gridmaps 2000–2024; TRANS includes aviation and shipping.	https://edgar.jrc.ec.europa.eu/dataset_ghg2025
MEIC-China / MEIC-global-CO_2	Distinct products and geographical supports. Historical national/sector data are used only where verified as compatible.	http://meicmodel.org.cn
CEDS (v2024_04_01 in data pipeline)	Annual country/sector historical CO_2 series; an input to the annual constraints, not an independent validation; no monthly profiles. Sector-specific process matches are evaluated only where an explicit source correspondence is available.	https://www.pnnl.gov/projects/ceds
Li et al. (2026) daily CO_2	14 countries/regions (11 geographical series matched to MCR sectors); power, industry, residential and transport (including aviation), 1970–2024. Historical monthly lineage overlaps EDGAR.	https://doi.org/10.6084/m9.figshare.28827932
ODIAC monthly fossil CO_2	High-resolution monthly fossil-fuel CO_2; used as allocation information where compatible and therefore not an independent comparison; not interchangeable with all anthropogenic CO_2 processes.	https://www.odiac.org

Dataset or variable	Role and provider	Official access or download URL
DMSP-OLS / VIIRS night time lights	Built-environment and human-activity spatial evidence for sector-specific 0.05° allocation; Earth Observation Group.	https://eogdata.mines.edu/products/vnl/
GHS-SMOD R2023A	Settlement morphology and urban spatial evidence for sector-specific 0.05° allocation; European Commission JRC.	https://human-settlement.emergency.copernicus.eu/ghs_smod2023.php
Population grid	Population-based spatial evidence for diffuse anthropogenic sectors; used only where sector-process compatibility is established.	-
Harmonised NDVI composite	Vegetation and agricultural spatial evidence used as a relative support covariate, not an emission-magnitude constraint; NOAA AVHRR/VIIRS CDR harmonised by the authors.	https://www.ncei.noaa.gov/products/climate-data-records/normalized-difference-vegetation-index
ERA5 total precipitation	Agricultural hydroclimatic spatial evidence used as a relative support covariate; Copernicus C3S/ECMWF.	https://cds.climate.copernicus.eu
GLASS BSA_SW albedo	Temporally compatible agricultural land-surface evidence used as a relative support covariate; Beijing Normal University.	https://glass-product.bnu.edu.cn
HILDA+ / ESA CCI–Copernicus C3S land cover	Land-use and sector-eligibility evidence, especially for agriculture.	https://landuse.sites.uu.nl/datasets/hilda ; https://cds.climate.copernicus.eu
GRIP4 total road density	Road-density evidence for land transport; GLOBIO/PBL.	https://www.globio.info
gROADS v1	Mapped terrestrial roads. Source release and reference-year limitations are considered during predictor screening.	https://sedac.ciesin.columbia.edu/data/set/groads-global-roads-open-access-v1
Global Carbon Grid / GID	0.10° gridded point-source-related emissions (2019 reference); facility coordinates are not implied by its nominal resolution.	https://gidmodel.org.cn/?page_id=1425
CAMS EGG4 (XCO_2 and atmospheric CO_2)	Atmospheric column and concentration diagnostic context only; not a direct emission truth and not used as an emission-magnitude or allocation constraint.	https://ads.atmosphere.copernicus.eu/datasets/cams-global-ghg-reanalysis-egg4-monthly

Full-coverage fields use a regular 0.05° grid in geographic coordinates (EPSG:4326), comprising 7200 × 3600 cells globally. The reconstruction spans 672 months from January 1970 to December 2025. Direct monthly gridded sector information is concentrated in 2000–2024. Earlier patterns combine available historical inventories with suitable geographical and seasonal information. Figure 2 distinguishes annual records, national monthly series and gridded inputs.

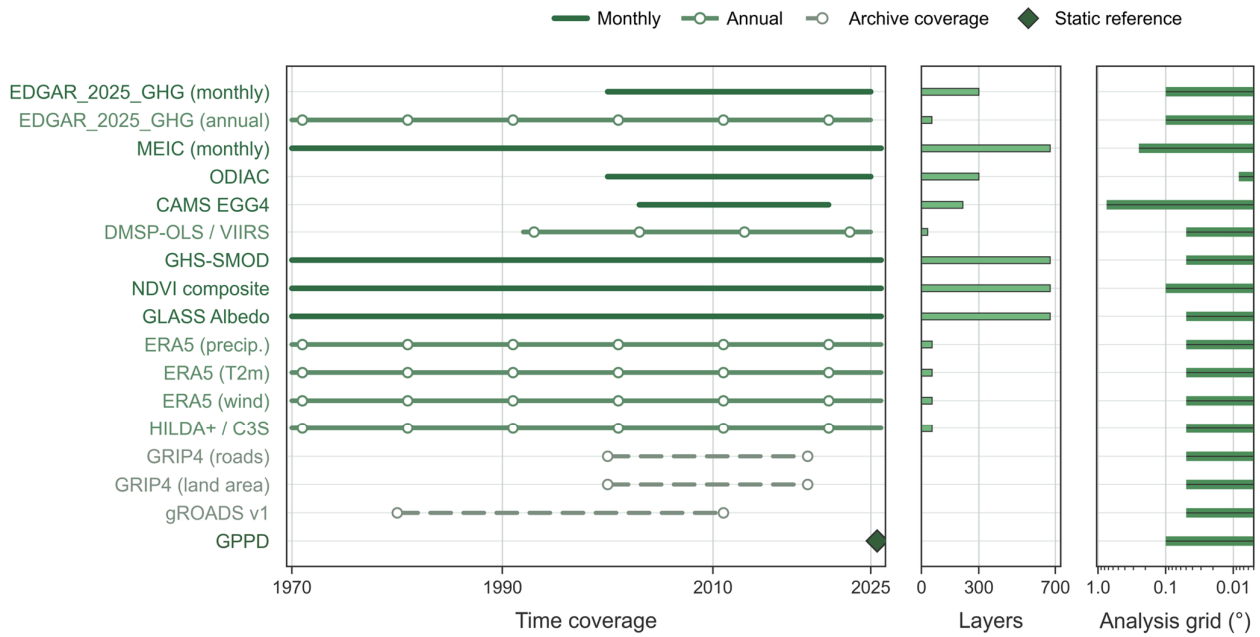


Figure 2. Temporal availability of the emission inventories and spatial predictors used in MCR-CO_2. Symbols distinguish directly available monthly records, annual information and spatial datasets applied to historical reconstruction.

The inventory resolves seven terrestrial sectors, with aviation and shipping distributed separately and counted once in combined totals. EDGAR's broader monthly transport aggregate includes aviation and navigation, so it is not interchangeable with terrestrial Transport. Industrial combustion, industrial processes and fuel-related activities are assigned by emitting process rather than source label. Agriculture and Waste cover specified anthropogenic CO_2 processes and exclude CH_4, N_2O and ecosystem carbon exchange. Table S1 lists EDGAR source category codes and exclusions. Comparisons with CEDS, Li et al. and MEIC use corresponding processes.

Annual estimates are compared on common geographical and accounting domains to assess emission magnitude and historical evolution (Fig. 3). Differences are interpreted in relation to source data, system boundaries and activity assumptions. Agreement with a contributing inventory provides a consistency check rather than an independent accuracy estimate.

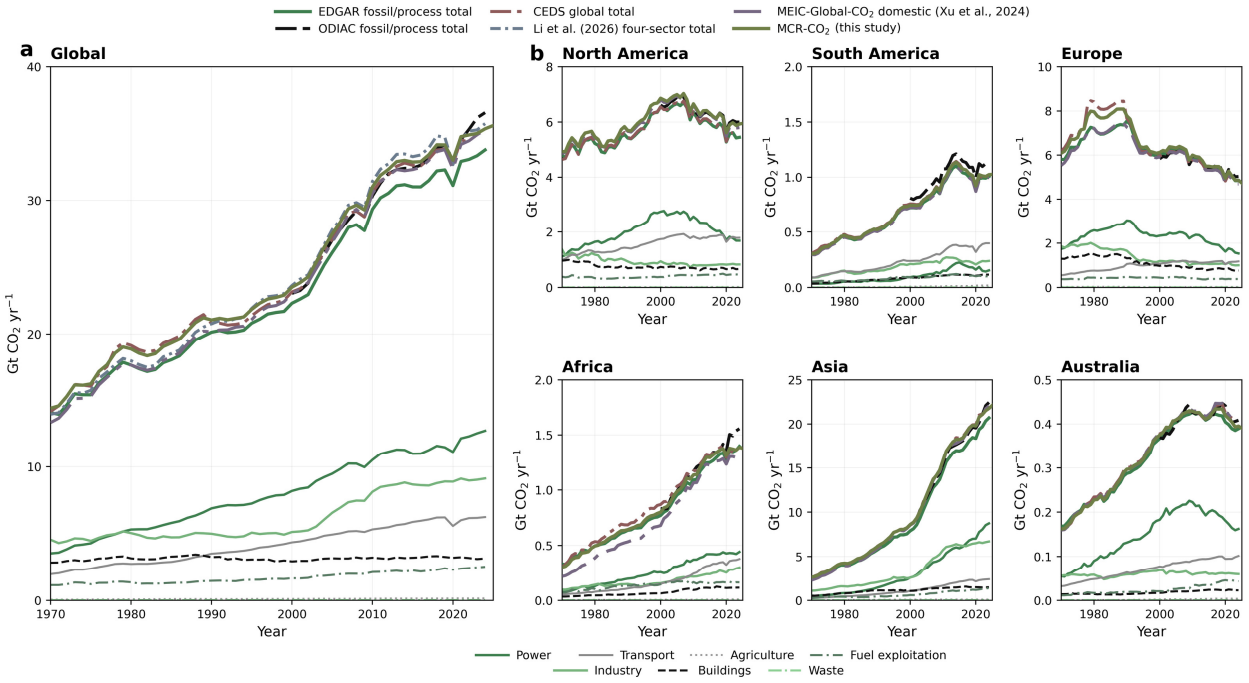


Figure 3. Global and regional annual anthropogenic CO_2 emissions compared across MCR-CO_2 and available reference inventories. Curves are interpreted according to each source's geographical and sectoral coverage.

Quantitative comparisons match gases, years, regions and emitting processes wherever source category codes permit. Unmatched processes are excluded rather than assigned zero emissions. Terrestrial Transport excludes the separately reported aviation and shipping components. Agricultural and waste-related CO_2 is not interchanged with CH_4, N_2O or ecosystem carbon exchange. These compatibility rules apply throughout the annual and monthly evaluations.

2.2 Annual emission calibration

Annual country–sector totals are estimated after aligning geographical and process coverage. Here, c, s, y and d index country, sector, year and source inventory. Source-specific log anomalies are expressed relative to a reference year, with a numerical stabiliser εA (Eq. 1). Temporal regularisation describes their evolution (Eq. 2), and source weights combine the fitted slopes (Eq. 3). Calibration therefore reflects compatible source histories rather than a single global correction factor.

$$R_{c,s,y}^{(d)} = \ln\left(\frac{A_{c,s,y}^{(d)}+\epsilon_A}{A_{c,s,y_{\mathrm{ref}}}^{(d)}+\epsilon_A}\right) \quad (1)$$

Source-specific anomalies are combined only on years and categories with suitable information. Temporal regularisation limits unsupported jumps while allowing documented changes in energy demand, industrial activity and fuel use. The resulting annual totals therefore reflect the available source histories rather than a uniform scaling of the global EDGAR series (Eq. 2).

$$R_{c,s,y}^{(d)} = \alpha_{c,s}^{(d)} + b_{c,s}^{(d)}(y - y_{\mathrm{ref}}) + \varepsilon_{c,s,y}^{(d)} \quad (2)$$

The resulting country–sector trajectories inform annual calibration factors that vary by country, sector and year and are bounded between 0.50 and 2.00. These factors change annual mass while retaining normalised monthly fractions and inherited spatial support. Compatible MEIC estimates contribute to Power, Industry, Buildings, Fuel and terrestrial Transport where available. Its agriculture and forestry fuel-use category is not treated as the entire agricultural CO_2 sector. Figure S4 evaluates annual differences on comparable source–sector supports.

$$b_{c,s} = \frac{\sum_{d\in\mathcal{D}_{c,s}^{A}} \rho_{c,s}^{(d)} b_{c,s}^{(d)}}{\sum_{d\in\mathcal{D}_{c,s}^{A}} \rho_{c,s}^{(d)}} \quad (3)$$

The magnitude and direction of differences between the resulting sector totals and the source inventories are quantified over 1970–2024. Signed annual differences and their absolute distributions across available comparable source-year

pairs are presented in Fig. S4. These statistics describe disagreement among emission estimates, including shared methodological influences; they do not identify one source as the true value.

For 2025, we carry forward the latest supported calibration relationship for each country and sector, usually that of 2024. The retained factor is applied to reconstructed 2025 monthly and spatial fields; the twelve monthly emissions are not copied from 2024. The final year is therefore a model-based extension with less direct source support than preceding years. Subsequent releases can replace inherited factors and seasonal guidance while retaining the grid, units and sector definitions.

2.3 Monthly emission reconstruction

Monthly emissions are represented by twelve non-negative fractions of each positive annual country–sector budget, with the fractions summing to one. Compatible EDGAR national monthly series are used throughout their historical coverage; the shorter 2000–2024 interval describes the available gridded monthly sector maps, not the full history of monthly evidence. Li et al. (2026) and selected MEIC records provide further temporal guidance. CEDS informs annual budgets but is not treated as a separate measurement of monthly seasonality. Equations (4)–(7) describe estimation and normalisation.

Let A denote the annual emission total for country c, sector s and year y, and let q(c,s,y,m) be the fraction attributed to month m. For a positive annual total, the fractions sum to one; a year with no annual emissions remains zero. Missing source values remain missing rather than being treated as observed zero emissions (Eq. 4).

$$q_{c,s,y,m}^{(d)} = \frac{M_{c,s,y,m}^{(d)}}{\sum_{k=1}^{12} M_{c,s,y,k}^{(d)}} \tag{4}$$

To estimate monthly profiles consistently, the twelve shares are represented by eleven log-ratio coordinates and transformed back to a non-negative composition (Eq. 5). This representation respects the requirement that all monthly fractions sum to one. Numerical stabilisation is restricted to the estimation procedure and does not introduce emissions into genuinely zero annual totals.

$$\ell_{c,s,y,m}^{(d)} = \log\left(\frac{q_{c,s,y,m}^{(d)} + \epsilon_q}{q_{c,s,y,12}^{(d)} + \epsilon_q}\right) \tag{5}$$

A regularised hierarchical model combines the available monthly evidence across source, country, sector and year while retaining sector-dependent differences. The model accounts for uneven coverage and overlapping source histories, so close agreement with an input inventory is not interpreted as independent validation. Its formulation is given in Eq. (6).

$$\ell_{c,s,y,m}^{(d)} = \mu_{s,m} + u_{c,s,m} + \left(b_{s,m} + v_{c,s,m}\right)(y - y_0) + \varepsilon_{c,s,y,m}^{(d)} \tag{6}$$

Observed monthly information informs the reconstructed fractions wherever its coverage and process definitions allow. Elsewhere, the hierarchical model transfers suitable seasonal information across countries, sectors or years under regularisation. Land cover, precipitation and settlement variables chiefly constrain plausible emitting locations; they are not treated as direct measurements of agricultural or waste CO_2 seasonality. Every monthly composition is normalised before it is multiplied by the calibrated annual budget.

The temporal record contains 360 months before 2000, 300 months during 2000–2024 and 12 model-extended months in 2025. All reconstructed years satisfy the monthly sum constraint. Continuity across the transition to the modern monthly gridded record is examined in the retrospective diagnostics, although continuity alone does not demonstrate the accuracy of historical seasonality.

Output GeoTIFF stacks store integer tonnes of CO_2 per cell per month. The value −2147483648 represents missing data and is distinct from a valid emission value of zero. Rounding errors and agreement between sector totals and aggregate rasters are checked after integer conversion; these numerical checks are separate from tests of the reconstructed seasonal or geographical patterns.

$$E_{c,s,y,m}^{T} = A_{c,s,y}^{\mathrm{MCR}}\, \hat{q}_{c,s,y,m} \tag{7}$$

Retrospective tests compare the reconstructed monthly fractions with compatible withheld records. The baselines are equal allocation across the twelve months and the mean seasonal composition of the fitting period. Source-withholding experiments measure changes in monthly-share RMSE; separate country and historical-window results show when the transferred mean performs as well as, or better than, the reconstruction (Fig. S3; Table 3). Shared upstream activity information means that these are conditional retrospective tests rather than fully independent observations of every historical month.

2.4 Spatial predictors

Spatial predictors were selected by emitting process. Power plants and industrial sites inform concentrated sources, roads inform terrestrial Transport, and settlements and building activity inform Buildings. Extraction and processing infrastructure guides Fuel. Agricultural land and environmental variables identify plausible support for the covered agricultural CO_2 processes. They do not measure individual liming, urea or combustion emissions. Population and settlements likewise provide indirect Waste indicators rather than facility observations. Figure 12 quantifies dependence on each predictor family.

Spatial datasets differ in reference year, coverage and effective resolution. Predictors are screened for geographical coverage, temporal suitability and redundant information before allocation. Where contemporaneous observations are unavailable, transferred geographical information is identified as reconstructed support. Figure 4 illustrates associations among inventory fields and spatial predictors.

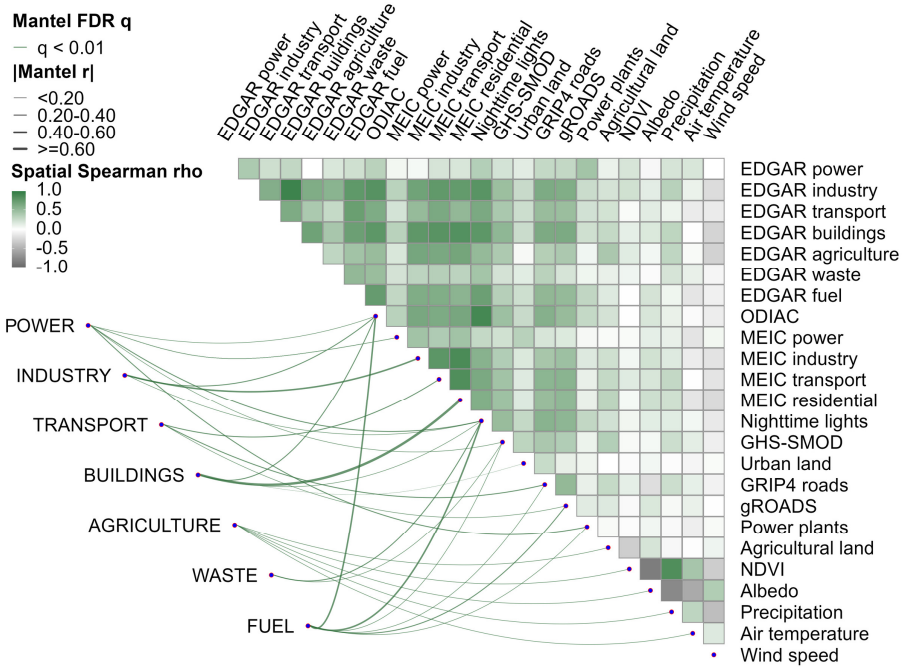


Figure 4. Spatial associations among the inventory and predictor datasets used for allocation. The correlations and network links describe shared geographical patterns.

A point-source field supplied at 0.10° identifies activity within a parent cell but cannot resolve its four 0.05° children. Allocation uses finer geographical evidence through non-negative, normalised scores. A positive reconstructed child cell represents modelled placement rather than a surveyed facility. Historical use of recent predictors is treated as reconstruction. CAMS EGG4 column CO_2 supplies diagnostic atmospheric context and is excluded from emission targets and allocation weights.

Annual country–sector totals constrain magnitude, monthly shares determine timing, and spatial weights distribute each monthly amount over eligible cells. Subsequent support redistribution conserves the country–sector–month budget. Figure 1 links these inputs, reconstruction stages and conservation checks.

2.5 Spatial allocation and mass conservation

Each monthly 0.10° parent-cell budget is allocated to four 0.05° children using non-negative, sector-specific spatial weights. Eligible predictors, including compatible ODIAC information, determine relative shares. Normalisation conserves the prescribed parent emission mass (Eqs. 8–11).

Candidate spatial variables are rescaled using lower and upper reference bounds and clipped to the interval from zero to one (Eq. 8). The resulting scores identify plausible allocation locations rather than observed emission rates.

$$z_{s,r,t}(j) = \mathrm{clip}\left(\frac{g_{s,r}\left(x_{r,t}(j)\right) - Q^{L}_{s,r,t}}{Q^{U}_{s,r,t} - Q^{L}_{s,r,t} + \epsilon_z},\ 0,\ 1\right) \tag{8}$$

Available predictor scores are combined using sector-specific weights and normalised over valid predictor information (Eq. 9). A 0.10° source constrains its parent cell; finer evidence is needed to distinguish the children. Predictor families are withheld in turn to quantify their influence on the resulting spatial shares (Fig. 12).

$$S_{s,j,t} = \frac{\sum_{r \in \mathcal{R}_{s,j,t}} \omega_{s,r} z_{s,r,t}(j)}{\sum_{r \in \mathcal{R}_{s,j,t}} \omega_{s,r}} \quad (9)$$

Combined scores are converted to weights and normalised over eligible child cells within each 0.10° parent (Eq. 10). When eligible scores vanish, a mass-conserving fallback distributes the parent budget without activating excluded or NoData cells. True-zero annual totals remain zero, and missing inputs remain missing. Numerical stabilisers do not authorise new emitting support. The separate support-transfer step conserves country–sector–month mass rather than unchanged parent-cell totals.

$$E_{s,j,t}^{0.05^\circ} = M_{s,p,t}^{0.10^\circ} \frac{e_{s,j,t}\left(S_{s,j,t}+\epsilon_S\right)^{\kappa_S}}{\sum_{\ell \in C(p)} e_{s,\ell,t}\left(S_{s,\ell,t}+\epsilon_S\right)^{\kappa_S}} \quad (10)$$

The effect of individual predictor families is evaluated by removing each family and recomputing child-cell weights while holding the parent mass unchanged. This mass-preserving test measures dependence on input geographical information (Fig. 12).

For every monthly parent cell, the sum of the four children equals the prescribed mass. A separate redistribution step, when applied, may transfer emissions between parent cells but conserves the country–sector-month total. The accounting domains and their independent conservation checks are defined in Eq. (11).

Conservation is checked at three scales: within each 0.10° parent during four-child disaggregation, within each country, sector and month after permitted transfers between parents, and between exported sectoral and aggregate GeoTIFFs. Transfers do not cross country boundaries. True zero emissions, unavailable source information and cells selected as eligible recipients are kept distinct. Integer rounding is evaluated separately from the conservation constraints applied before the final conversion to stored whole tonnes (Eq. 11).

$$\sum_{j \in C(p)} E_{s,j,t}^{0.05^\circ} = M_{s,p,t}^{0.10^\circ} \quad (11)$$

2.6 Reconstruction of emitting locations

An additional support-adjustment step considers eligible cells with zero emissions in the initial allocation. A long short-term memory (LSTM) model evaluates sequences of spatial activity predictors and assigns candidate support scores. Eligibility rules and acceptance thresholds guide bounded transfers from existing emitting cells within the same country, sector and month (Eqs. 12–18). Operational transfers apply only to Agriculture and terrestrial Transport. The monthly transferred pools represent 2.2–4.0% of global Agriculture mass and 1.0–2.0% of global Transport mass. Withdrawals do not exceed 5.5% of active donor mass.

The support-adjustment model is separate from annual calibration and monthly profile reconstruction. A candidate cell is not activated solely because a predictor such as night-time lights is present: the recurrent score, geographical eligibility and support thresholds must also be satisfied. The spatial model was fitted in the upstream reconstruction, while the subsequent annual emission calibration left its learned support configuration unchanged.

$$\mathbf{X}_{s,k,t} = \left[\mathbf{x}_{s,k,t-L+1}, \ldots, \mathbf{x}_{s,k,t}\right] \quad (12)$$

The availability of historical predictors limits the interpretation of recovered emitting locations. An illuminated area in a recent satellite record, for example, cannot establish the operation of a facility in 1970. Recovered support is therefore a modelled allocation hypothesis rather than a record of facility opening or closure.

The recurrent model was assessed through annual trajectories, training and validation loss, and held-out predictor permutation tests (Fig. S5). Kullback–Leibler divergence documents convergence and selected stopping epochs for seven fitted sector models. Permutation tests measure changes in spatial total-variation distance when predictor groups are disrupted. Seven-sector diagnostics are distinct from the operational support transfers, which are restricted to Agriculture and Transport. Accepted transfers retain the eligibility rules and mass constraints.

$$\mathbf{h}_{s,k,t} = \mathrm{LSTM}_{\theta_s}\left(\mathbf{X}_{s,k,t}\right) \quad (13)$$

Candidate cells are retained only when the predicted support and the corresponding sector mask both permit emission allocation (Eqs. 14–16). Cells that fail the combined criteria remain unchanged. The procedure thus constrains where redistribution is permitted but does not independently certify the presence of every newly represented emitter.

Accepted candidate locations receive bounded emission transfers taken from eligible existing donors. The distribution of those transfers is normalised to the accepted cells so that the amount removed from donors is exactly the amount added to recipients. The annual sector total consequently remains unchanged (Eqs. 14–18).

$$p_{s,k,t} = \sigma\left(\mathbf{w}_s^{\mathrm{T}} \mathbf{h}_{s,k,t} + b_s\right) \quad (14)$$

A cell without valid emission support cannot receive transferred mass. Where no candidate meets the screening criteria, the redistribution is zero and the initial field is retained.

$$g_{s,k,t} = \mathbb{I}\left(E^{\text{base}}_{s,k,t} = 0\right)\mathbb{I}\left(p_{s,k,t} \geq \tau_s\right)\mathbb{I}\left(S_{s,k,t} \geq S^{\min}_s\right)\mathbb{I}\left(e_{s,k,t} = 1\right) \quad (15)$$

A normalised destination distribution is evaluated only when accepted support scores are positive. If the denominator is zero or no eligible candidate is available, the transfer is suppressed. Numerical stabilisation does not create positive emissions in otherwise inadmissible cells.

$$\pi_{c,s,k,t} = \frac{g_{s,k,t} p^{\gamma_s}_{s,k,t} \left(S_{s,k,t} + \epsilon_S\right)^{\eta_s}}{\sum_{j \in c_{c,s,t}} g_{s,j,t} p^{\gamma_s}_{s,j,t} \left(S_{s,j,t} + \epsilon_S\right)^{\eta_s}} \quad (16)$$

The amount removed from emitting donor cells is bounded by their original mass. The corresponding gains in destination cells sum to exactly the withdrawn quantity, conserving the country–sector-month budget (Eq. 17).

$$E^{*}_{c,s,k,t} = E^{\text{base}}_{c,s,k,t} - \beta_{c,s,t} M^{\text{base}}_{c,s,t} d_{c,s,k,t} + \beta_{c,s,t} M^{\text{base}}_{c,s,t} \pi_{c,s,k,t} \quad (17)$$

After support adjustment, conservation is checked for the corresponding country, sector and month. The stored raster totals are also inspected for integer rounding effects, which are distinct from the physical question of whether modelled emitting locations are geographically correct.

National boundaries, coastlines, valid zeros and missing cells are distinguished throughout the support adjustment. This prevents redistribution across countries or into excluded spatial cells (Eq. 18).

$$\sum_{k \in c} E^{*}_{c,s,k,t} = M^{\text{base}}_{c,s,t} \quad (18)$$

2.7 Evaluation methods

Evaluation addresses annual accounting, monthly seasonality, spatial placement and uncertainty. Historical source comparisons assess sector differences over 1970–2024 (Figs. 3 and S4). Monthly source-withholding tests use equal-month and fitting-period-mean baselines (Fig. S3; Tables 2 and 3). Predictor-removal experiments isolate geographical input dependence at fixed parent mass (Fig. 12). Regional benchmarks assess spatial agreement (Fig. S2). Source configurations measure annual and monthly sensitivity, while separate Monte Carlo simulations propagate an annual-budget uncertainty component (Fig. S6; Tables 4 and 5).

The regional comparison uses common geographical masks and the same Power, Industry, Buildings and Fuel bundle for MCR-CO_2 and EDGAR. References are CAMS-REG for Europe in 2023, Vulcan V4 for the conterminous United States in 2022, and ODIAC for three 2024 domains. The reference maps retain their available fossil-emission totals, so sector coverage is not identical to the four-sector bundle. Metrics therefore assess spatial pattern concordance under these accounting differences. They include JSS, log-scale correlation, normalised RMSE, hotspot overlap and centroid displacement. CAMS-REG is described by Kuenen et al. (2022). Fixed-parent-mass experiments in Figs. 12 and S6i isolate allocation sensitivity.

Figure S6 combines historical diagnostics with distinct annual, monthly and spatial assessments. Panels (a–f) describe temporal variability and geographical composition, panels (g–i) assess sensitivity, and panel (j) reports conditional annual-budget uncertainty.

2.8 Sensitivity to annual sources, monthly profiles and spatial allocation

We evaluated 400 configurations using annual estimates and monthly profiles from compatible MCR-CO_2, EDGAR, CEDS, Li et al. and MEIC records. Alternatives were screened for gas, emitting process, units, country, sector and year. Source selections were held consistent by sector over time. Unavailable matches retained the MCR-CO_2 estimate rather than introducing unsupported replacements. Each annual total was redistributed using non-negative monthly fractions summing to one. The configurations therefore measure sensitivity to the tested sources while preserving annual accounting.

Annual departures from MCR-CO_2 were summarised by their median and 2.5th and 97.5th percentiles for six periods. These are 1970–1980, 1981–1990, 1991–2000, 2001–2010, 2011–2019 and 2020–2025. Monthly sensitivity is the maximum absolute change among twelve monthly shares, expressed in percentage points. A separate spatial test compares native allocation with uniform allocation among eligible children within each 0.10° parent in June 2024 regional windows. Parent and country masses remain fixed. Total variation distance (TVD) measures the fraction of mass reassigned spatially. Table 4 reports these sensitivities and compatible-source coverage.

The 400 configurations are source combinations rather than independent observational realisations. Their percentile ranges describe the portion of the reconstruction covered by compatible alternatives. The spatial TVD similarly measures allocation sensitivity in the selected windows. These tests complement the probabilistic annual-budget experiment in Sect. 2.9 without being treated as a joint error distribution.

2.9 Propagation of annual-budget uncertainty

We performed a separate Monte Carlo experiment using the CO_2-specific global IPCC-category uncertainty bounds reported by Solazzo et al. (2021, Table 6). Their 2015 bounds were transferred to MCR-CO_2 country–sector budgets as a reference model, rather than treated as measured country-specific uncertainties. Table 5 gives the category mapping. Mixed industrial combustion and process emissions were assigned the higher IPPU benchmark, with an Energy-only alternative reported in Table S3.

For each of 1,000 realisations, a positive lognormal multiplier was assigned to every country–sector pair and held fixed over 1970–2025 (Eq. 19). The main case uses fully shared within-sector country errors ($\rho = 1$). Alternatives use $\rho = 0$ and 0.5; different sectors are independent in all cases. The sector-common and country–sector terms are independent standard normal variates, and the random seed is 20261026.

$$F_{c,s}^{(b)} = \exp[\mu_s + \sigma_s(\sqrt{\rho}\, Z_s^{(b)} + \sqrt{1-\rho}\, Z_{c,s}^{(b)})] \quad (19)$$

Lognormal parameters match the lower and upper fractional reference bounds at the 2.5th and 97.5th percentiles (Eq. 20). Φ^{-1} denotes the standard normal quantile. This endpoint-matching parameterisation does not force the multiplier median or mean to one, so simulated medians need not coincide with the baseline.

$$\mu_s = \frac{\ln(1+l_s) + \ln(1+u_s)}{2},\ \sigma_s = \frac{\ln(1+u_s) - \ln(1+l_s)}{2\,\Phi^{-1}(0.975)} \quad (20)$$

Each multiplier scales its annual budget and the corresponding country–sector emission field (Eq. 21). Monthly fractions q and final spatial fractions w remain fixed and normalised. Existing donor withdrawals and recipient gains scale together, preserving the within-country accounting constraints in every realisation. The conditional relative annual-budget uncertainty therefore passes directly to each positive monthly grid cell (Eq. 22). True-zero emissions remain zero.

$$A_{c,s,y}^{(b)} = F_{c,s}^{(b)}\, A_{c,s,y},\ E_{c,s,y,m,j}^{(b)} = F_{c,s}^{(b)}\, E_{c,s,y,m,j} \quad (21)$$

$$\mathrm{Var}(E \mid q,w) = (qw)^2\, \mathrm{Var}(A),\ u_{rel}(E \mid q,w) = u_{rel}(A) \quad (22)$$

We summarised sector totals by central 95% Monte Carlo intervals for the six periods in Sect. 2.8 and the full record. Computation uses the country-assigned annual table rather than resampling the rasters. These intervals quantify the transferred annual-budget component conditional on fixed monthly profiles, spatial weights and support decisions. The 400 source configurations separately characterise temporal and source-choice sensitivity; spatial perturbations assess allocation dependence.

3 Data record and emission patterns

3.1 Dataset structure

MCR-CO_2 is distributed as monthly GeoTIFF stacks on a regular 0.05° WGS84 grid (EPSG:4326) for January 1970–December 2025. Seven stacks represent Power, Industry, terrestrial Transport, Buildings, Fuel, Agriculture and Waste. Aviation and shipping are separate layers. Each stack contains 672 chronologically ordered bands. Full-global layers comprise 7200 × 3600 cells; Waste retains its native extent of 180° W–180° E and 60° S–85° N. Values are integer tonnes of CO_2 per cell per month, with NoData distinct from valid zeros.

Annual and monthly products can be obtained by summing the appropriate bands and sectors, subject to the distinction between terrestrial emissions and the separate aviation and shipping components. The fine-grid spatial distribution is illustrated in Fig. 5, and the temporal behaviour of representative countries is shown in Fig. 6. All sums must respect the native validity mask of the waste layer.

3.2 Global and regional emissions

Terrestrial CO_2 emissions increase from 15.140 Gt in 1970 to 25.387 Gt in 2000, 33.856 Gt in 2010 and 39.075 Gt in 2024. They reach 39.385 Gt in 2025, approximately 2.60 times the 1970 level. Aviation contributes 1.130 Gt and shipping 0.864 Gt to the reported 2025 combined total of 41.380 Gt CO_2, with components rounded separately. Terrestrial emissions decline from 37.672 Gt in 2019 to 36.580 Gt in 2020, then rebound to 38.306 Gt in 2021. Figure 5 distinguishes concentrated urban and industrial centres from diffuse sources.

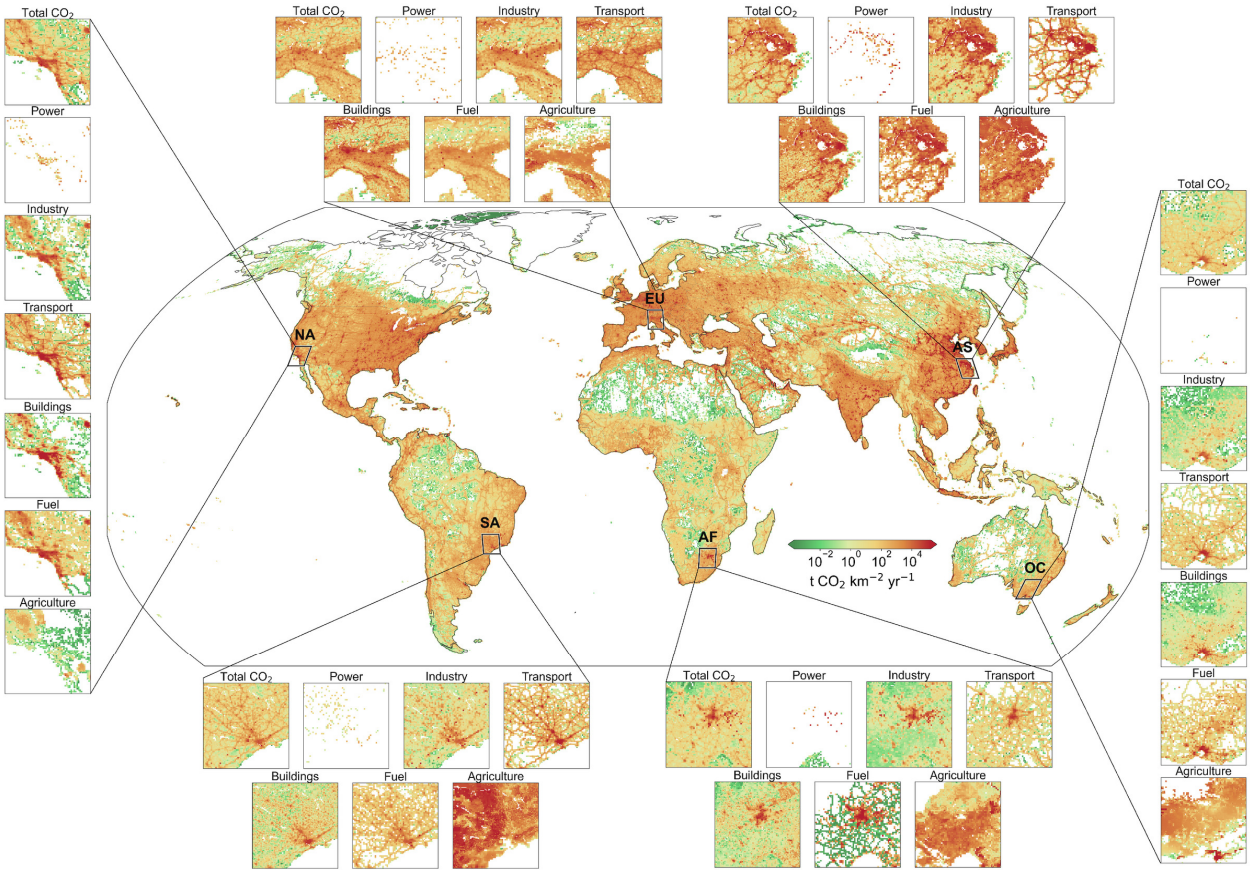


Figure 5. Annual anthropogenic CO_2 emission density in 2024 at 0.05°, expressed in t CO_2 km^{-2} yr^{-1}. Regional panels show total emissions and selected terrestrial sectors in North America, Europe, Asia, South America, Africa and Oceania.

National monthly series reveal contrasting emission histories and seasonal patterns (Fig. 6). Power and Industry emissions increased substantially in China and India, while several European countries show declines in recent decades. Russia and Ukraine show pronounced decreases in the early 1990s. Stacked series retain the seven terrestrial sectors and their within-year variation.

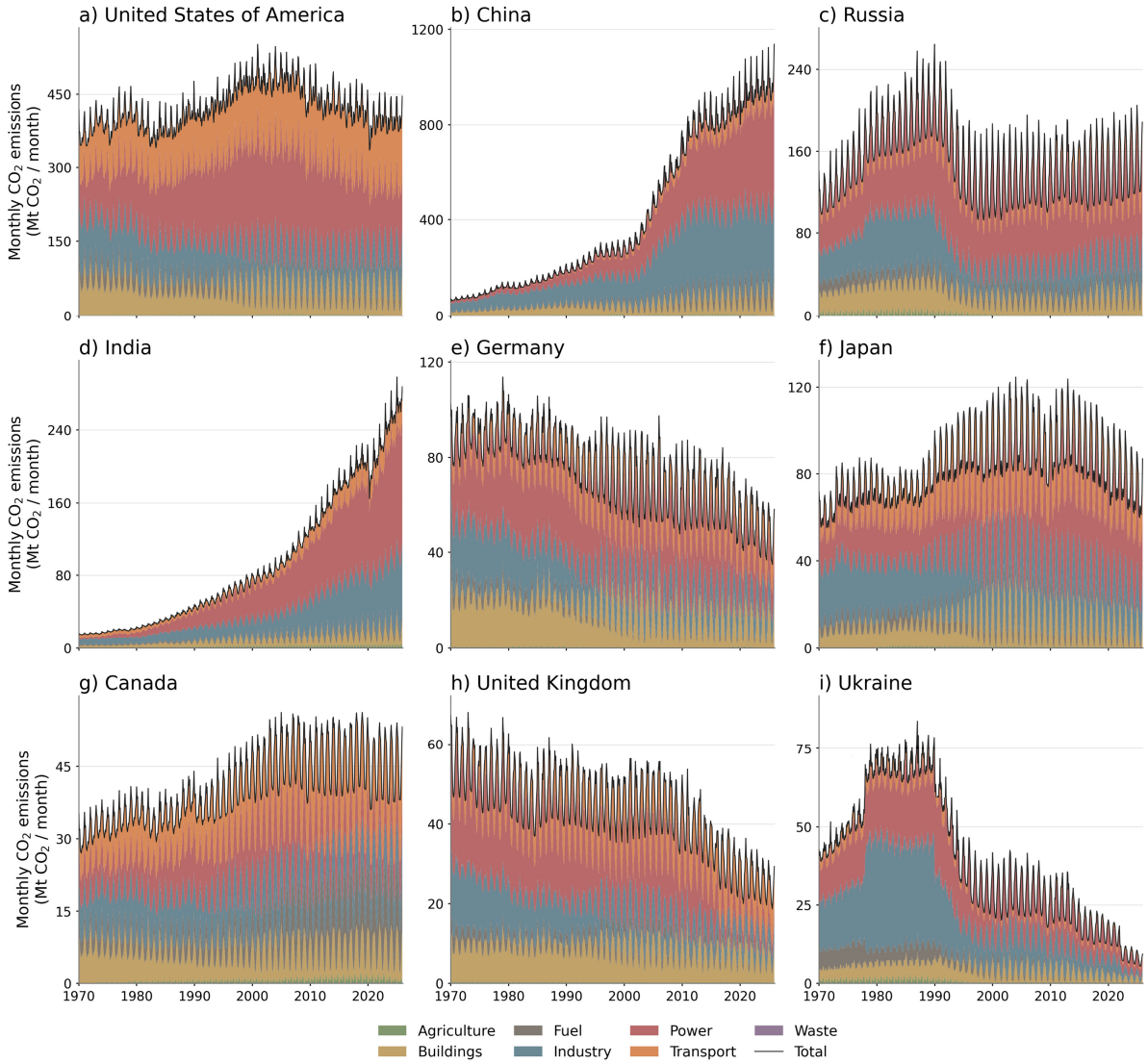


Figure 6. Monthly terrestrial-sector CO_2 emissions in nine countries during 1970–2025, expressed in Mt CO_2 $month^{-1}$. Stacked series show seven sectors and the black line their total. Aviation and shipping are excluded.

3.3 Spatial emission patterns

The 0.05° fields resolve urban development, industrial clusters, transport networks and other eligible emission sources. Figure 7 compares MCR-CO_2 and EDGAR in 1980 and 2024 for Agriculture in Bolivia, Buildings in Benelux–Randstad, Transport in Africa, Industry in the Yangtze River Delta, and Waste in the northeastern United States. Land-use and satellite layers provide geographical context. Positive cells created through support redistribution remain modelled locations rather than confirmed facilities.

Differences between final MCR-CO_2 and EDGAR maps reflect both calibrated emission budgets and the distribution of mass within the output grid (Fig. 13). Figure S2 evaluates the resulting spatial fields against CAMS-REG, Vulcan and ODIAC in defined geographical domains; these comparisons describe the performance of the full products. Figure 12 then isolates the contribution of individual spatial predictor groups by removing them while preserving prescribed emission mass. The fixed-mass comparison in Fig. S6 provides a further test of how strongly fine-grid placement depends on allocation choices.

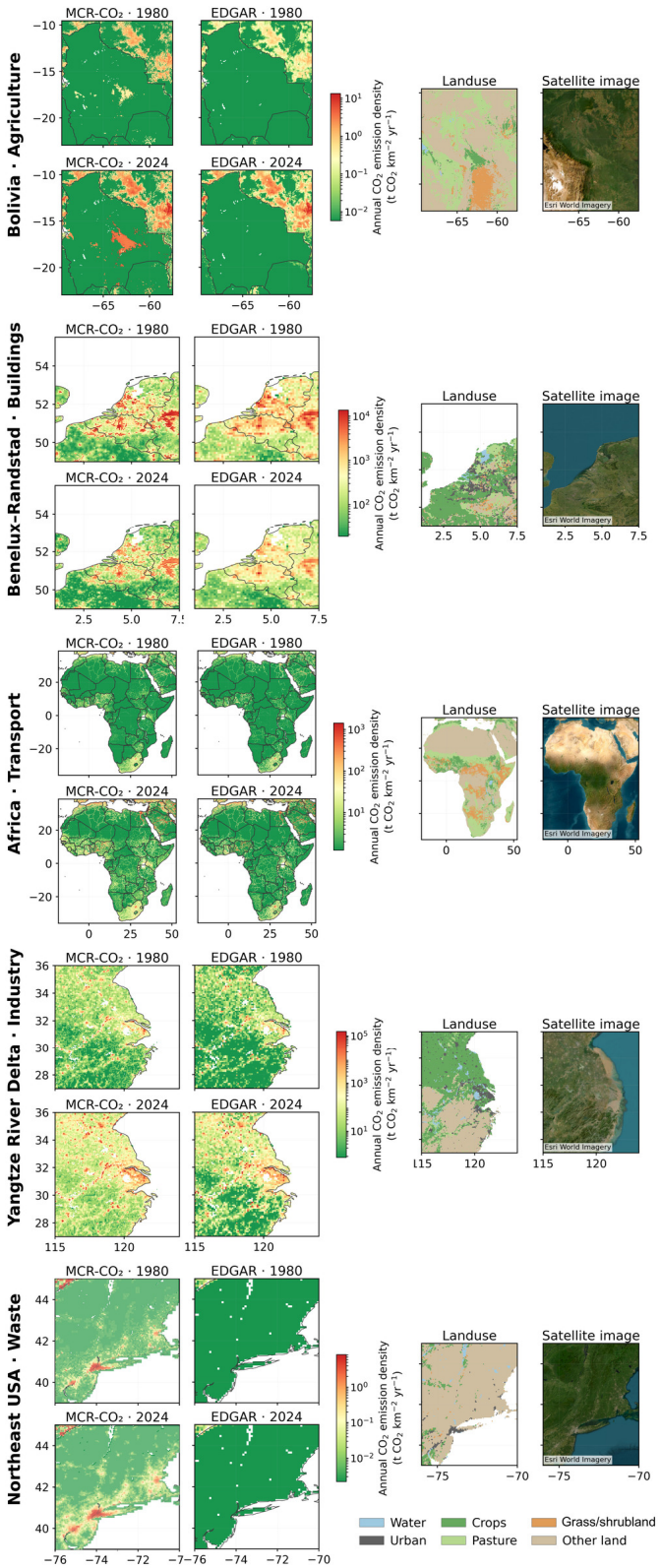


Figure 7. Annual sectoral CO_2 emission density from MCR-CO_2 and EDGAR in 1980 and 2024 for five regional examples. Each example uses a common colour scale across both inventories and years, in t CO_2 km^{-2} yr^{-1}; ranges differ among examples. Land-use layers and satellite imagery provide geographical context. The maps show allocation differences rather than independent verification of individual emitters.

4 Evaluation

Evaluation combines inventory consistency, retrospective monthly tests, regional spatial comparisons and controlled perturbations. Contributing inventories assess compatibility, while CAMS-REG and Vulcan provide distinct

regional benchmarks. Source-choice and predictor-removal tests measure sensitivity. The Monte Carlo experiment adds a separately parameterised annual-budget uncertainty component (Figs. 8–14 and S2–S6; Tables 2–5).

4.1 Monthly inventory consistency

Daily Li et al. (2026) estimates are aggregated to monthly totals after matching geography and emitting processes. The comparison spans 660 months during 1970–2024 across 11 geographical series (Fig. 8). It assesses consistency over a wide emission range. Shared upstream information is considered when interpreting agreement alongside the conditional retrospective tests.

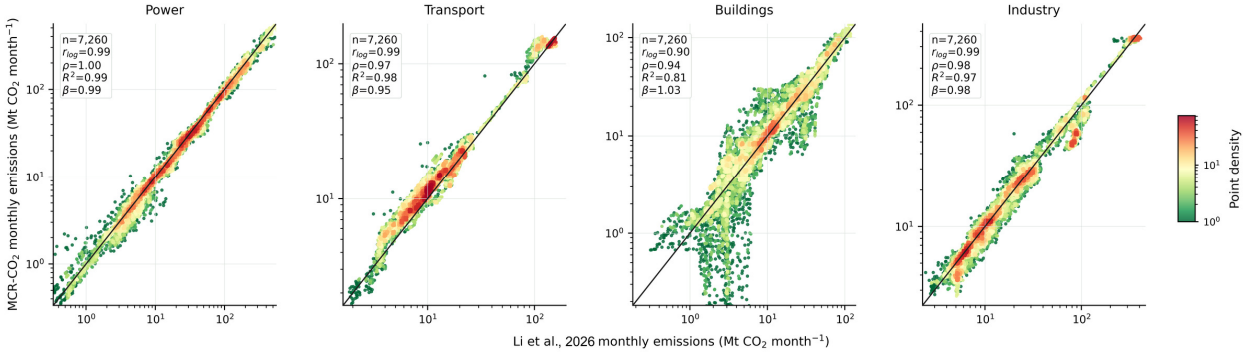


Figure 8. Monthly country–sector emission estimates from MCR-CO₂ and Li et al. (2026) on common temporal and geographical support. Each sector is compared over 660 months across 11 series. These comparisons assess inventory consistency.

4.2 Annual inventory consistency

The comparisons with CEDS confirm that MCR-CO₂ follows the broad historical evolution of the major fossil-emission sectors, particularly Power, Industry and terrestrial Transport (Fig. 9). The most pronounced departures are associated with narrower sector definitions. Waste, for example, has a weak log-scale correlation of 0.16 and a fitted slope of 0.13 against CEDS; the fitted Fuel slope is 0.36. These statistics describe differences between inventory categories, not a loss of accuracy established by independent observations. A scope audit explains the weak Waste agreement: CEDS 5C waste combustion is a broader category than EDGAR Waste (median CEDS/EDGAR ratio 23.46; r = 0.309), whereas the scope-matched EDGAR WASTE_INC series reproduces EDGAR Waste exactly (r = 1.000, slope 1.000). Differences in the treatment of fossil and biogenic CO₂, waste processes and fuel transformation help explain why like-for-like process matching is essential. The comparisons in Fig. S4 further show the sign and extent of differences on common source support. Because CEDS also informs the reconstruction, Fig. 9 is used as evidence of inventory consistency rather than independent validation.

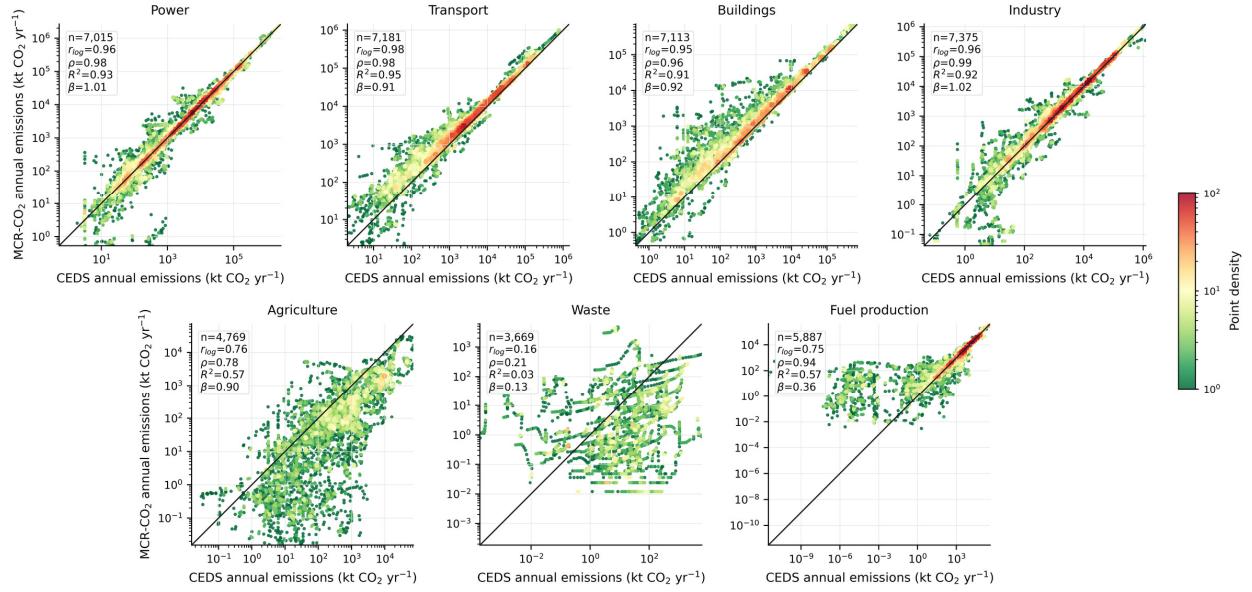


Figure 9. Annual country–sector CO_2 estimates from MCR-CO₂ and CEDS on the available matched categories and years. Each panel reports a log-scale association and fitted relationship, which describe agreement between inventory estimates rather than accuracy against an independent observation.

Comparison with MEIC likewise shows close correspondence across the main emitting activities where geography, period and process definitions match (Fig. 10). Power generation, Industry and terrestrial Transport exhibit broadly

comparable emission levels and temporal patterns. Greater dispersion is concentrated in selected Buildings and Agriculture comparisons, where the available MEIC products and MCR-CO_2 do not always represent the same emitting processes. In particular, the narrower agricultural fuel-use category in MEIC cannot be treated as a direct estimate of all anthropogenic agricultural CO_2. The separate China and global MEIC products are therefore interpreted according to their respective coverage, without conflating differences in inventory scope with demonstrated reconstruction error.

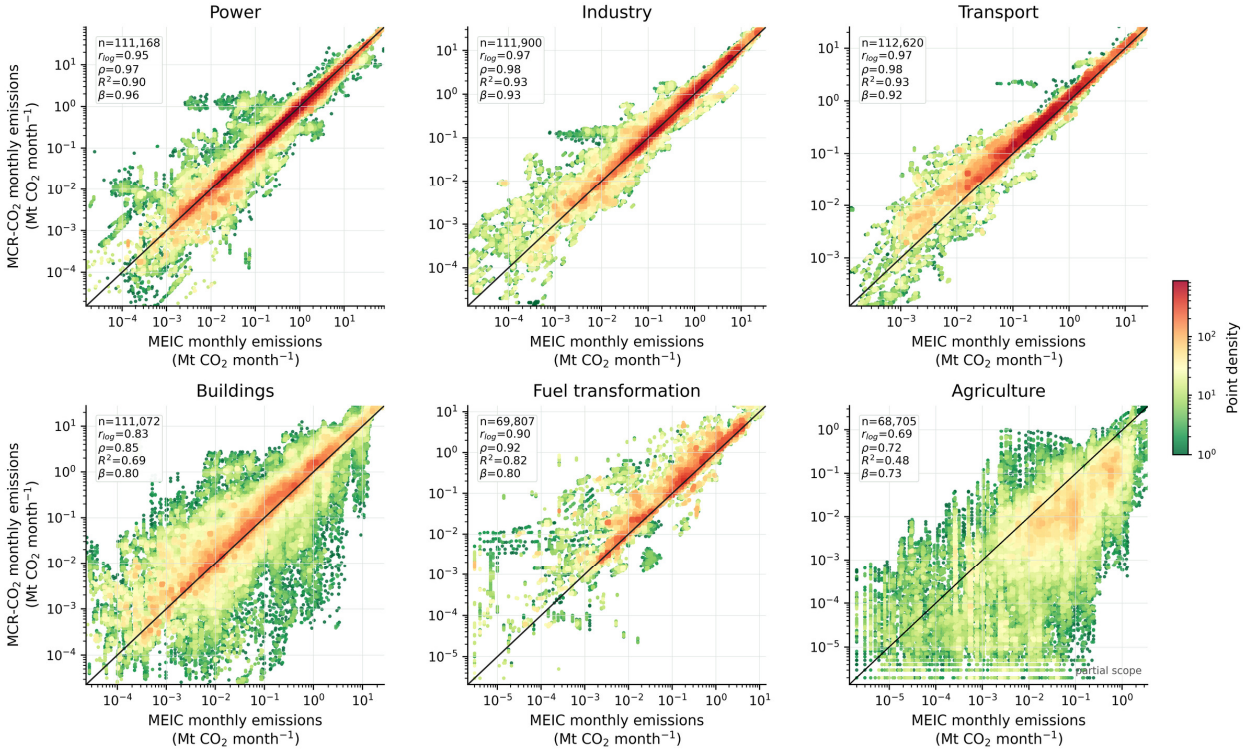


Figure 10. Monthly sectoral emission estimates compared with MEIC on the available common source, temporal and geographical coverage.

Figure S4 compares annual sector estimates from the available inventories over matched periods and source categories. Overall correspondence is strongest for the dominant fossil-fuel sectors, whereas Agriculture and Waste exhibit a wider spread between inventory definitions and treatment of their included processes. This distinction is also visible in the global sector-share ratios in Fig. 14b. The sectoral comparison therefore reinforces the importance of harmonised process definitions rather than suggesting that one dataset must reproduce the allocation of every other inventory.

4.3 Historical monthly reconstruction

Historical monthly reconstruction was evaluated using annual-normalised twelve-month profiles. Baselines comprise equal monthly allocation and the mean seasonal composition transferred from a fitting period. Source-withholding tests identify contributions from EDGAR, MEIC and Li et al. Country and five-year results examine changing performance across the 1970s, 1980s and 1990s (Fig. S3; Tables 2 and 3).

$$p_{m,y} = \frac{E_{m,y}}{\sum_{k=1}^{12} E_{k,y}} \tag{23}$$

Monthly reference profiles are drawn from suitable dated source series. Daily Li et al. values are aggregated to monthly totals, and the ODIAC time series provides fossil-emission context where relevant. CEDS contributes annual historical information but not direct monthly reference profiles. Years with undefined monthly fractions are excluded rather than converted to observed zero-emission months.

Seasonal agreement is evaluated using Jensen–Shannon similarity (JSS), monthly-share RMSE, Pearson correlation, seasonal amplitude and peak timing. JSS compares annual-normalised twelve-month compositions. These complementary metrics describe monthly shape rather than independently validating annual emission magnitude (Eqs. 23–28).

Monthly composition is better resolved when similarity, error and seasonal amplitude are considered together. For the matched Li et al. (2026) comparison, JSS rises from 94.99% before 2000 to 98.95% after 2000, while monthly-share RMSE falls from 0.987 to 0.212 percentage points (Table 2). These results indicate closer agreement in the later period, although high similarity between nearly uniform monthly profiles does not necessarily imply accurate recovery of seasonal peaks.

$$\mathrm{JSS}(q,r) = 100\left[1 - \frac{\mathrm{JSD}(q,r)}{\ln(2)}\right] \quad (24)$$

$$\mathrm{JSD}(q,r) = \frac{1}{2}\sum_m q_m \ln\left(\frac{q_m}{u_m}\right) + \frac{1}{2}\sum_m r_m \ln\left(\frac{r_m}{u_m}\right) \quad (25)$$

$$u_m = \frac{q_m + r_m}{2} \quad (26)$$

$$\mathrm{RMSE}_{pp} = 100\sqrt{\frac{1}{12}\sum_{m=1}^{12}(p_m - q_m)^2} \quad (27)$$

RMSE is expressed in percentage points of the annual emission share. Normalised seasonal errors are interpreted only where the reference has meaningful amplitude. Annual totals are evaluated separately, and comparisons without a defined seasonal pattern do not receive arbitrary phase scores.

$$A(q) = 100\left[\max_m(q_m) - \min_m(q_m)\right] \quad (28)$$

Seasonal amplitude is the maximum minus minimum monthly share, expressed in percentage points (Eq. 28). Phase describes dominant seasonal timing where sufficiently defined. High similarity between nearly uniform profiles is interpreted alongside amplitude and correlation.

The source experiments separately omit EDGAR, Li et al. and MEIC from the relevant monthly reconstruction diagnostic. Their change in root mean square error (RMSE) is positive when retaining the source improves the prediction and negative when the excluded source is unhelpful in the tested setting. The historical and recent source effects are shown in Fig. S3a, b, while the direct comparison with the two baselines appears in Fig. S3c, d.

Reconstruction skill varies across the ten evaluated countries and successive five-year historical windows. Industry, Fuel and Agriculture show small positive median gains over the transferred fitting-period mean in some windows; Power, Buildings and Transport have weaker or negative differences elsewhere (Fig. S3e, f). A single transferred profile is therefore not equally suitable for every sector and decade.

At the boundary between historical reconstruction and modern gridded monthly inputs around 2000, the reconstructed global monthly profiles maintain 99.39% Jensen–Shannon similarity. This high continuity indicates a smooth transition between periods and supports the consistency of the monthly series as the source record changes.

Withholding individual sources provides a more direct measure of their contribution. Before 2000, excluding Li et al. increases median monthly-share RMSE for Buildings by 0.425 percentage points across 23 matched cases; excluding MEIC increases the Industry error by 0.136 points across 213 cases. After 2000, excluding EDGAR increases the Agriculture error by 1.008 points across 164 cases (Table 3). The gains differ by sector, but show that suitable monthly records can add information beyond a transferred seasonal mean.

Historical-window medians differ from the transferred-mean baseline by at most about 0.02 percentage points, with gains and losses depending on sector (Fig. S3f). These small median differences temper the stronger source-withholding results: the monthly series is internally mass-conserving, but historical seasonal accuracy depends on which evidence is available and on the reconstruction period.

Table 2. Agreement of reconstructed monthly emission profiles with available temporal reference inventories. Metrics describe monthly composition, seasonal variability and correlation on common temporal coverage.

Comparison source	Period	N years	JSS (%)	RMSE (pp)	Seasonal nRMSE	Pearson r	Amplitude ratio (external/MCR)
Li et al. (2026)	Pre-2000	30	94.99	0.987	2.749	0.968	0.292
Li et al. (2026)	Post-2000	25	98.95	0.212	0.529	0.992	0.073
ODIAC	Post-2000	25	96.75	0.646	1.626	0.859	0.316
MEIC	Pre-2000	30	99.07	0.186	0.273	0.956	0.190
MEIC	Post-2000	25	96.27	0.738	1.150	0.611	1.378
EDGAR	Post-2000	25	96.33	0.731	2.345	0.999	0.052

The seasonal statistics provide additional detail about these patterns. JSS measures the overall monthly composition, Pearson correlation identifies whether the peaks and troughs occur together, and amplitude ratios show whether the reference seasonality is stronger or weaker. Li et al. has a post 2000 Pearson correlation of 0.992 with MCR-CO_2 on the

matched supports, while ODIAC has 0.859 and MEIC varies between the historical and modern comparisons (Table 2). Figure 11 illustrates the associated monthly profiles; Table S2 extends the same diagnostics across geographical regions.

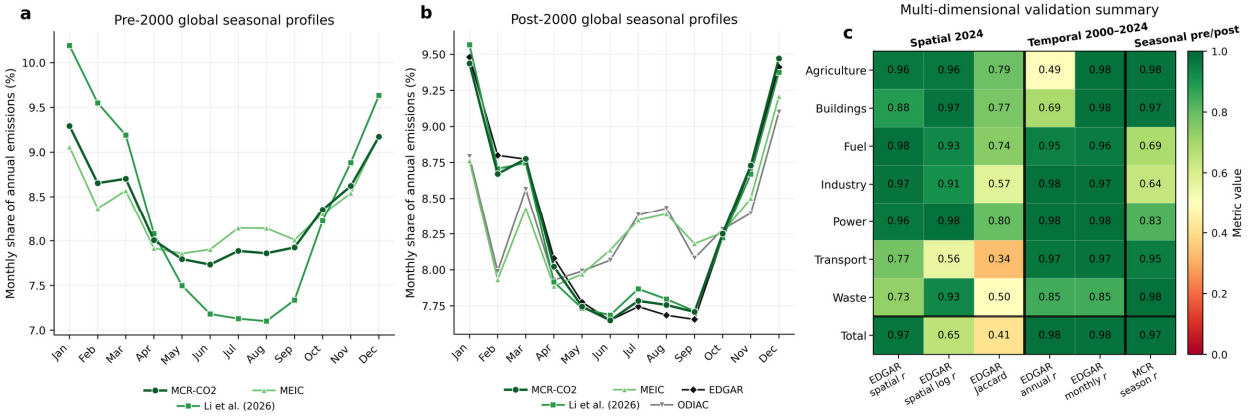


Figure 11. Annual-normalised monthly emission profiles and continuity of reconstructed seasonality. Each monthly value is a fraction of its country–sector annual total; similarity, error and amplitude metrics assess the twelve-month composition and should not be interpreted as errors in annual emission magnitude.

Across continents, seasonal similarity is generally high on available comparable source histories, while amplitude and correlation remain more variable. This is expected because two monthly distributions can assign similar average shares yet represent different seasonal peaks. Table S2 therefore reports all the composition, error, correlation and amplitude indicators, allowing users to distinguish stable seasonal fractions from stronger country or sector-specific variation.

Table 3. Change in monthly-share RMSE after withholding individual inventory sources. Positive values indicate lower error when the corresponding source is included; case counts refer to matched country-reference comparisons.

Period	Sector	Removed source	Country–reference cases	Median ΔRMSE (pp)
Pre-2000	Buildings	Li	23	+0.425
Pre-2000	Industry	MEIC	213	+0.136
Pre-2000	Power	MEIC	213	+0.106
Post-2000	Agriculture	EDGAR	164	+1.008
Post-2000	Buildings	EDGAR	419	+0.071
Post-2000	Industry	EDGAR	427	+0.018
Post-2000	Waste	EDGAR	133	+0.000

4.4 Spatial evaluation

We quantified the influence of each family of geographical predictors by removing it from the spatial model and recomputing the 0.05° distribution while keeping the prescribed emissions in every 0.10° parent cell unchanged (Fig. 12). This design reveals the additional geographical structure associated with power facilities, road networks, settlements and other sector-specific evidence. It tests the contribution of those predictors directly, without confusing the effect of finer spatial placement with a change in the country or sector emission budget. The resulting sector differences are consistent with the stronger geographical concentration of some emitting activities.

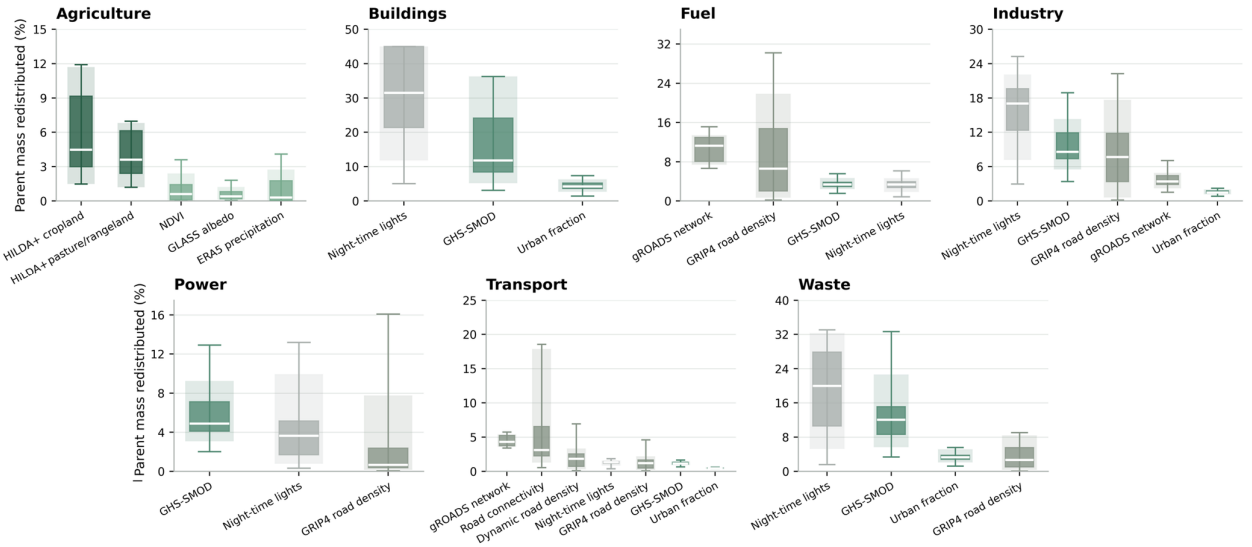


Figure 12. Spatial allocation sensitivity to sector-specific predictor families. Each perturbation withholds the indicated predictor group and recomputes 0.05° child-cell shares while retaining the same 0.10° parent emission mass.

In the two domains with distinct regional benchmarks, MCR-CO_2 improves overall spatial similarity relative to EDGAR (Fig. S2). Against CAMS-REG in Europe (2023), JSS rises from 46.2% to 48.0% and log-scale correlation from 0.763 to 0.797; nRMSE falls from 10.976 to 8.957. Hotspot overlap increases from 0.500 to 0.516, although centroid displacement rises from 159 to 224 km. Against Vulcan V4 in the conterminous United States (2022), JSS increases from 37.6% to 47.8%, correlation from 0.768 to 0.814 and hotspot overlap from 0.474 to 0.572. The corresponding nRMSE decreases from 10.345 to 9.942 and displacement from 50 to 46 km. The two benchmarks thus support better distributional agreement while retaining metric-specific differences. Because these native-product comparisons combine differences in annual budget and in placement, the fixed-mass tests in Fig. 12 and Fig. S6i are used to isolate the sensitivity of placement.

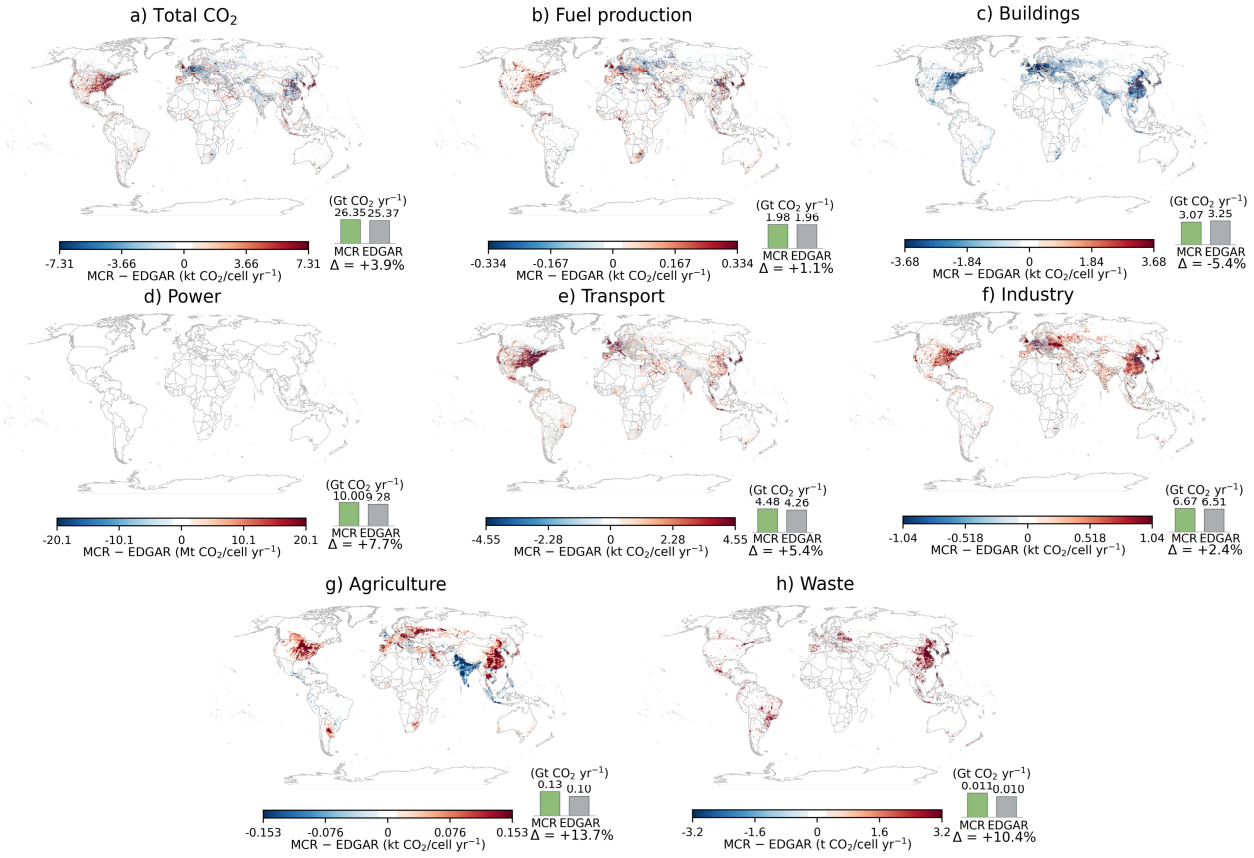


Figure 13. Differences between annual MCR-CO_2 and EDGAR emission fields on comparable spatial support. Mapped differences combine changes in the calibrated emission magnitude with changes in fine-scale distribution.

ODIAC provides a further, although not independent, comparison in three 2024 domains (Fig. S2). Relative to EDGAR, MCR-CO_2 increases JSS from 27.7% to 30.2% in Brazil, 31.2% to 47.4% in southern Africa and Madagascar, and 28.4% to 41.8% in Australia. nRMSE falls from 41.140 to 34.655 in southern Africa and Madagascar and from 30.295 to 24.541 in Australia. In Brazil, however, nRMSE increases from 13.182 to 17.467 despite higher JSS; Australian top-decile hotspot overlap also declines from 0.368 to 0.357. These mixed local-error results are important when interpreting improvements in overall spatial similarity.

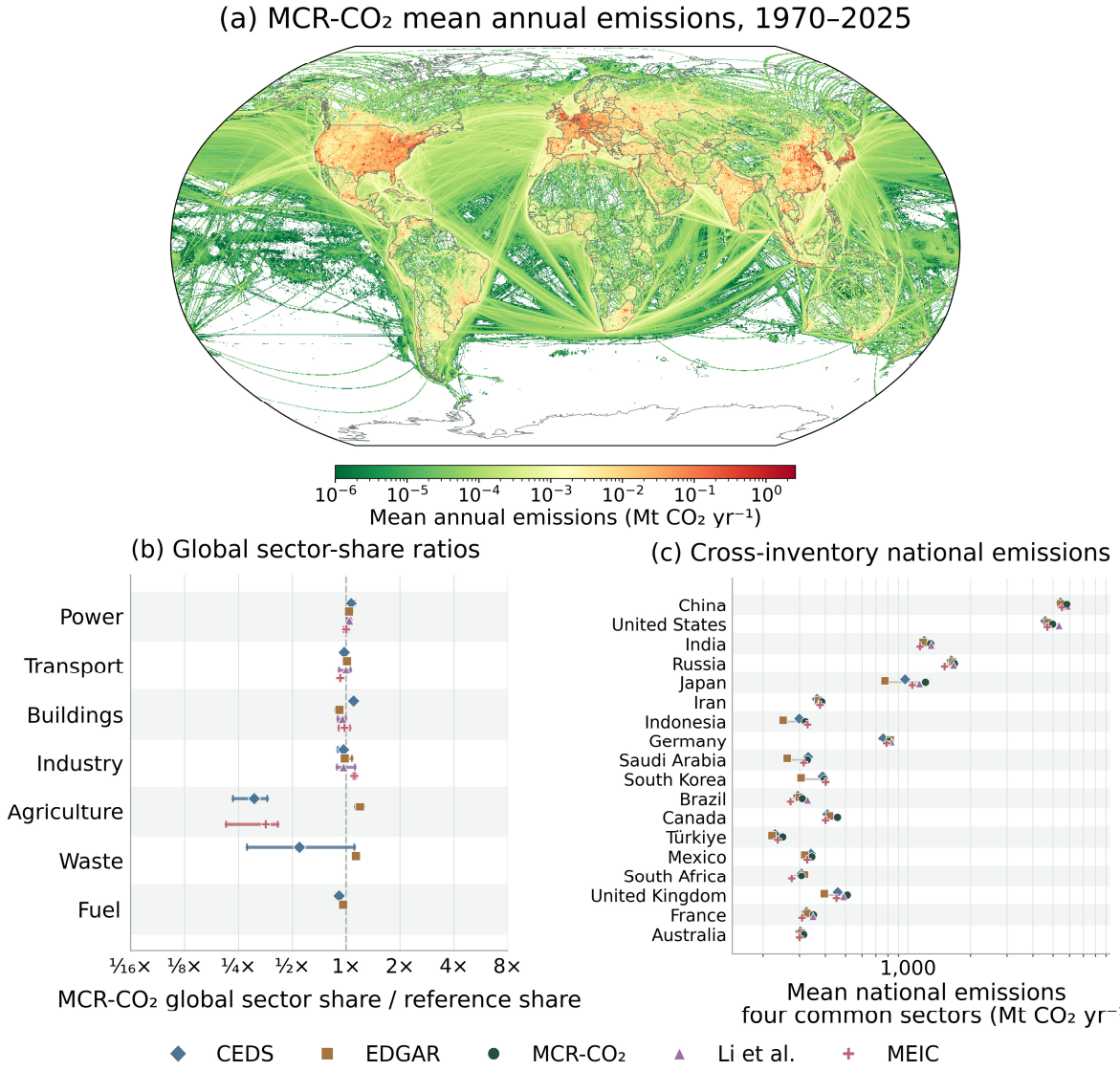


Figure 14. Global patterns and cross-inventory comparisons of MCR-CO_2. (a) Mean annual spatial distribution over 1970–2025. (b) Ratio of each MCR-CO_2 global terrestrial sector share to the corresponding reference-inventory sector share; a ratio of one indicates identical shares, and ratios are not direct comparisons of absolute sector emissions. Markers show the available CEDS, EDGAR, Li et al. and MEIC comparisons on their reported supports. (c) Mean national emissions for common sectors in the countries shown. Cross-inventory differences should be interpreted with the corresponding sector and geographical coverage in mind.

Figure 14b provides a useful perspective on sector composition. Power, Transport, Buildings and Industry cluster close to a sector-share ratio of one across the available references, consistent with the close overall correspondence of the major fossil-emission categories. Agriculture is more distinct: its MCR-CO_2 share lies substantially closer to the EDGAR comparison than to the larger shares associated with the available CEDS and MEIC estimates. Waste also varies appreciably across inventory definitions, particularly in comparison with CEDS, although the EDGAR-aligned Waste category provides a more directly comparable process basis. The differences are concentrated in categories where emission accounting is especially sensitive to the activities included; they do not represent an equivalent discrepancy throughout the inventory. Independently of the cross-inventory comparison, sectoral and aggregate GeoTIFF totals pass the stated mass-conservation checks, including the treatment of Waste's shorter native geographical extent.

4.5 Source sensitivity and propagated annual-budget uncertainty

Historical annual comparisons show the largest contrasts in Agriculture and Waste, where process definitions differ most strongly (Fig. S4). Figure S6a–f complements these comparisons with interannual variability, seasonality and geographical concentration. Together, these diagnostics describe the structure of the record without treating variability across years as an error estimate.

The 400 compatible source configurations produce sector-dependent responses (Fig. S6g, h; Table 4). In 2020–2025, annual Agriculture departures range from −4.13% to +6.73%, compared with −0.49% to +0.12% for Power. The upper monthly-share shift reaches 0.738 percentage points for Buildings and 0.050 for Power. Industry and Transport generally show negative annual departures. These ranges quantify source-choice sensitivity on the available compatible support.

Table 4. Sectoral sensitivity of MCR-CO_2 to annual source choice, monthly timing and spatial allocation. Annual ranges are the 2.5th to 97.5th percentile deviations from the MCR-CO_2 baseline across 400 compatible source configurations in 2020–2025, in percent. Monthly shifts are the median to 97.5th percentile of the maximum absolute change among twelve monthly emission shares, in percentage points, over the same period. Spatial TVD measures the percentage of emission mass redistributed by a uniform alternative within eligible 0.10° parents in the selected North American window in June 2024. Source support is the largest fraction of reconstructed emission mass with a compatible annual alternative from any individual reference inventory in 2020–2025; the four columns therefore refer to explicitly different supports.

Sector	Annual range (%)	Monthly shift (pp)	Spatial TVD (%)	Source support (%)
Power	-0.49 to +0.12	0.023 to 0.050	64.6	8.8
Industry	-2.59 to +0.00	0.012 to 0.026	50.4	6.8
Transport	-1.61 to +0.00	0.035 to 0.090	7.8	20.2
Buildings	-0.82 to +0.43	0.047 to 0.738	28.2	14.2
Agriculture	-4.13 to +6.73	0.042 to 0.058	4.4	6.7
Waste	-0.21 to +0.00	0.000 to 0.003	20.1	0.2
Fuel	-1.81 to +0.54	0.002 to 0.018	16.4	9.9

The fixed-mass experiment in Fig. S6i shows how much geographical detail is contributed by the native allocation. In the selected North American window in June 2024, replacing predictor-informed placement with uniform distribution among eligible 0.05° cells produces a total variation distance of 64.6% for Power and 50.4% for Industry, compared with 7.8% for Transport and 4.4% for Agriculture (Table 4). All of these alternatives retain the prescribed 0.10° parent mass. The substantial differences for Power and Industry demonstrate that the fine-grid predictors materially shape the location of emissions, especially for concentrated activities; these are sensitivity measurements rather than errors relative to observed emission sources.

Source-choice sensitivity is modest for the dominant fossil-emission categories, but compatible alternatives cover different fractions of their mass. The largest single-source support in 2020–2025 ranges from 0.2% for Waste to 20.2% for Transport (Table 4). Reporting this coverage prevents narrow source-choice ranges from being interpreted as complete uncertainty bounds.

The Monte Carlo assessment adds a quantified annual-budget component distinct from source sensitivity (Fig. S6j; Table 5). In the main correlated case, central 95% intervals are approximately −7% to +7% for Power and Buildings, −7% to +8% for Transport and Fuel, −23% to +21% for Industry, −47% to +21% for Agriculture, and −39% to +24% for Waste. The rounded, visually estimated intervals are listed in Table 5. Identical relative intervals across the six periods follow from the time-invariant, sector-shared factors and do not imply equal empirical data quality across decades.

The annual table covers 233 countries or territories and 1,457 positive country–sector combinations over the record. Its country-assigned terrestrial sum is 35.869 Gt CO_2 in 2025, equivalent to 91.1% of the reported 39.385 Gt raster total. Monte Carlo aggregates are restricted to this assigned support; unassigned mass is excluded rather than given an implicit zero uncertainty. Aviation and shipping are outside this seven-sector experiment.

All seven 2020–2025 annual source-choice ranges in Table 4 are narrower than the conditional annual-budget intervals in Table 5. This comparison places the tested source sensitivity within a broader inventory-budget reference envelope. Different source coverage and perturbation models prevent interpretation as a decomposition of total reconstruction error. Correlation alternatives and the Industry mapping test make the dependence on aggregation assumptions explicit (Table S3).

Table 5. Transferred CO_2 uncertainty benchmarks and approximate central 95% Monte Carlo annual-budget intervals. Reference bounds are global IPCC-category values for 2015 from Solazzo et al. (2021, Table 6). Intervals are relative departures from country-assigned baseline sector mass for 1,000 realisations with $\rho = 1$ and seed 20261026. The same relative intervals apply to 1970–1980, 1981–1990, 1991–2000, 2001–2010, 2011–2019 and 2020–2025, and to the full record, by construction. They describe the annual-budget component conditional on fixed monthly and spatial fractions.

MCR-CO_2 sector	IPCC reference category	Transferred 95% bounds (%)	Monte Carlo 95% interval (%, approx.)
Power	Energy	±7.1	−7 to +7
Industry	IPPU	±22.5	−23 to +21
Transport	Energy	±7.1	−7 to +8
Buildings	Energy	±7.1	−7 to +7
Agriculture	Agriculture	±73.2	−47 to +21
Waste	Waste	±38.1	−39 to +24
Fuel	Energy	±7.1	−7 to +8

The 2025 estimates extend the reconstructed fields beyond the latest fully comparable gridded source years. Similarly, the earliest monthly patterns rely more heavily on transferred temporal information and geographical predictors than later decades. These differences in source availability should be considered when using the inventory for atmospheric modelling or historical attribution.

4.6 Recurrent model assessment

Figure S5 assesses the recurrent component through reconstructed annual sector trajectories, training and validation loss, and held-out predictor permutation tests. Stopping epochs follow validation behaviour, while the permutation analysis measures the change in spatial allocation when predictor families are disrupted. These diagnostics identify sector-dependent information in roads, settlements, night-time lights and related variables. They do not constitute independent confirmation of every candidate emitting location; the recurrent scores guide bounded redistribution of an existing emission budget.

Support adjustment only accepts locations that satisfy the geographical and sector eligibility rules, and the corresponding emission transfers remain within the same country, sector and month. Thus the recurrent component enhances spatial support while the annual and monthly budget remains defined by the harmonised inventories. Its validation and feature importance results complement the external geographical benchmarks and the allocation sensitivity analysis, offering an auditable description of the contribution of learned spatial patterns.

5 Discussion

MCR-CO_2 links long-term emission histories with the monthly and geographical detail needed in atmospheric and Earth system research. The contribution combines 672 months, seven terrestrial sectors and fine-grid allocation under common conservation rules. Separate aviation and shipping layers extend the record while preserving terrestrial-sector accounting. This integration makes uneven historical information usable within a consistent framework (Hoesly et al., 2018; Oda et al., 2018; Crippa et al., 2024).

The assessments identify where the reconstructed information adds value. Source-withholding experiments show measurable benefits from suitable monthly records, although gains over a transferred seasonal mean vary by sector and period. CAMS-REG and Vulcan comparisons support improved regional distributional agreement relative to EDGAR. Controlled spatial perturbations show that sector-specific predictors materially affect fine-grid placement. These results support use at the tested scales without equating every additional spatial feature with a verified emitter.

Differences among inventories are concentrated in process-sensitive categories. Agriculture and Waste require particular care because fuel use, liming, urea, incineration and biogenic CO_2 are grouped differently across products. Their larger discrepancies reinforce the value of the explicit crosswalk rather than implying equivalent disagreement across the dominant fossil sectors. Compatible process boundaries are therefore essential when comparing MCR-CO_2 with national totals or applying its sector fields.

The uncertainty assessment separates two practical questions. Source configurations show how annual budgets and monthly profiles respond to compatible inventory choices. The Monte Carlo experiment propagates an explicitly parameterised annual-budget component through the fixed monthly and spatial allocation. The resulting conditional intervals are broader than the tested annual source-choice ranges, placing that sensitivity in an inventory-uncertainty context. Country correlation and sector mapping remain explicit assumptions, making the comparison reproducible rather than treating inter-inventory spread as a probability model.

Interpretation depends on scale and source support. Regional benchmarks cover selected domains, and ODIAC contributes to allocation as well as comparison. Historical months and the 2025 extension rely more strongly on transferred information. Monte Carlo intervals describe annual-budget uncertainty on country-assigned support, conditional on fixed seasonal and spatial weights. They exclude additional profile, location and support-model errors. Within these boundaries, the record combines traceable budgets, evaluated seasonal reconstruction and geographically detailed emission fields for long-term analysis.

6 Conclusions

MCR-CO_2 provides 672 monthly anthropogenic CO_2 emission fields at 0.05° for 1970–2025 across seven terrestrial sectors, with aviation and shipping supplied separately. Terrestrial emissions rise from 15.140 Gt CO_2 in 1970 to 39.385 Gt in 2025. The 2025 total including aviation and shipping is 41.380 Gt CO_2. Annual budgets, monthly timing and geographical allocation remain distinct and are reconciled through explicit conservation checks.

The record combines sector-dependent gains in retrospective monthly reconstruction with improved spatial similarity against CAMS-REG and Vulcan relative to EDGAR. Source sensitivity, predictor-removal tests and conditional Monte Carlo propagation document complementary aspects of reliability. Historical coverage, monthly continuity, fine spatial detail and transparent accounting make MCR-CO_2 a useful foundation for atmospheric modelling and long-term emission assessment.

Code and data availability

The revised MCR-CO_2 dataset is deposited at https://doi.org/10.5281/zenodo.23337181 (Antezana Lopez, 2026a). Monthly GeoTIFF stacks are ordered from January 1970 to December 2025 and store tonnes of CO_2 per cell per month. Original reconstruction code and example fields are archived separately at https://doi.org/10.5281/zenodo.21523272 (Antezana Lopez, 2026b). The annual-budget propagation equations, uncertainty crosswalk and correlation assumptions used for this assessment are specified in Sect. 2.9 and Tables 5 and S3.

Author contributions

FPAL contributed to conceptualisation, data curation, formal analysis, methodology, software, validation, visualisation and the original draft. GZ contributed to conceptualisation, funding, resources, supervision and project administration. KZ, AC, AA, HJ and JLAL contributed to methodological review, interpretation and manuscript revision. All authors reviewed the manuscript.

Competing interests

The authors declare that they have no competing interests.

Disclaimer

Copernicus Publications remains neutral about jurisdictional claims made in the text, published maps, institutional affiliations, or any other geographical representation in this paper. While Copernicus Publications makes every effort to include appropriate place names, the final responsibility lies with the authors. Views expressed in the text are those of the authors and do not necessarily reflect the views of the publisher.

Acknowledgements

We thank the organisations that maintain the source emission inventories and ancillary datasets used in this study, including the European Commission Joint Research Centre (EDGAR and settlement products), the ODIAC development team, the Copernicus Climate Change and Atmosphere Monitoring Services, and the providers of land-use, road, night-time-light and environmental datasets. We also acknowledge institutional support from Beihang University and its Hangzhou International Innovation Institute.

Financial support

This research was supported by the National Natural Science Foundation of China (Grant No. 42471425).

References

Antezana Lopez, F. P.: MCR-CO_2 global monthly anthropogenic CO_2 emissions [data set], Zenodo, https://doi.org/10.5281/zenodo.23337181, 2026a.

Antezana Lopez, F. P.: Code and sample data for HBPG-CO_2 [code and data set], Zenodo, https://doi.org/10.5281/zenodo.21523272, 2026b.

Crippa, M., Guizzardi, D., Pagani, F., Schiavina, M., Melchiorri, M., Pisoni, E., Graziosi, F., Muntean, M., Maes, J., Dijkstra, L., Van Damme, M., Clarisse, L., and Coheur, P.: Insights into the spatial distribution of global, national

and subnational greenhouse gas emissions in the Emissions Database for Global Atmospheric Research (EDGAR v8.0), Earth Syst. Sci. Data, 16, 2811–2830, https://doi.org/10.5194/essd-16-2811-2024, 2024.

Dou, X., Hong, J., Ciais, P., Chevallier, F., Yan, F., Yu, Y., et al.: Near-real-time global gridded daily CO_2 emissions 2021, Sci. Data, 10, 69, https://doi.org/10.1038/s41597-023-01963-0, 2023.

European Commission Joint Research Centre: EDGAR_2025_GHG global greenhouse-gas emissions database, https://edgar.jrc.ec.europa.eu/dataset_ghg2025, release 2025 (accessed 17 October 2026).

Hoesly, R. M., Smith, S. J., Feng, L., Klimont, Z., Janssens-Maenhout, G., Pitkanen, T., Seibert, J. J., Vu, L., Andres, R. J., Bolt, R. M., et al.: Historical (1750–2014) anthropogenic emissions of reactive gases and aerosols from the Community Emissions Data System (CEDS), Geosci. Model Dev., 11, 369–408, https://doi.org/10.5194/gmd-11-369-2018, 2018.

Kuenen, J., Dellaert, S., Visschedijk, A., Jalkanen, J.-P., Super, I., and Denier van der Gon, H.: CAMS-REG-v4: a state-of-the-art high resolution European emission inventory for air quality modelling, Earth Syst. Sci. Data, 14, 491–515, https://doi.org/10.5194/essd-14-491-2022, 2022.

Li, T., Wang, L., Qiu, Z., Ciais, P., Davis, S. J., Deng, Z., Zhao, Y., Peters, G. P., Ke, P., Jones, M. W., et al.: Global daily CO_2 emissions from 1970 to 2024, Sci. Data, 13, 605, https://doi.org/10.1038/s41597-026-06621-9, 2026.

Oda, T., Maksyutov, S., and Andres, R. J.: The Open-source Data Inventory for Anthropogenic CO_2, version 2016 (ODIAC2016): a global monthly fossil fuel CO_2 gridded emissions data product for tracer transport simulations and surface flux inversions, Earth Syst. Sci. Data, 10, 87–107, https://doi.org/10.5194/essd-10-87-2018, 2018.

Solazzo, E., Crippa, M., Guizzardi, D., Muntean, M., Choulga, M., and Janssens-Maenhout, G.: Uncertainties in the Emissions Database for Global Atmospheric Research (EDGAR) emission inventory of greenhouse gases, Atmos. Chem. Phys., 21, 5655–5683, https://doi.org/10.5194/acp-21-5655-2021, 2021.

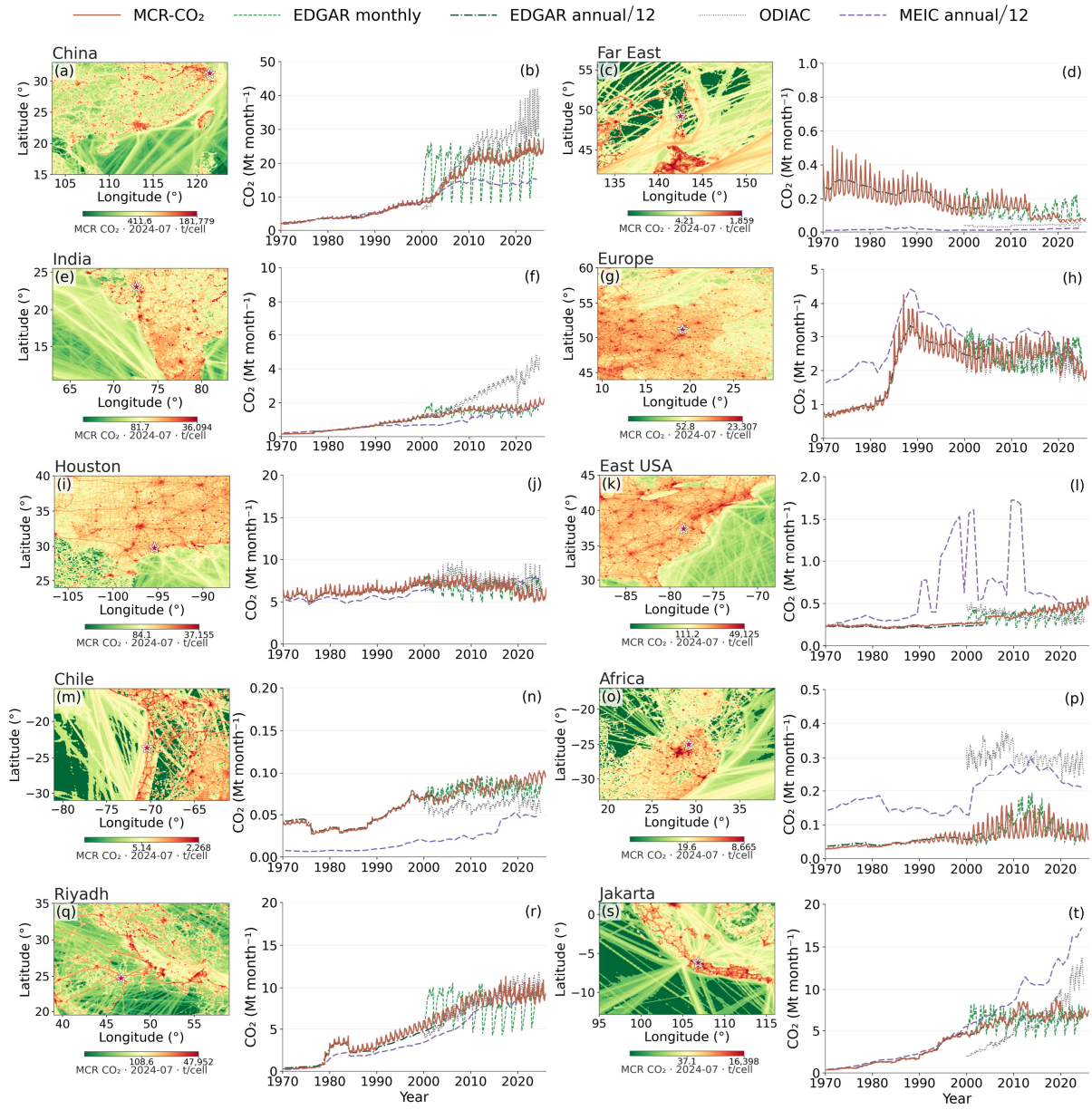
Xu, R., Tong, D., Xiao, Q., Qin, X., Chen, C., Yan, L., Cheng, J., Cui, C., Hu, H., Liu, W., Yan, X., Wang, H., Liu, X., Geng, G., Lei, Y., Guan, D., He, K., and Zhang, Q.: MEIC-global-CO_2: a new global CO_2 emission inventory with highly-resolved source category and sub-country information, Sci. China Earth Sci., 67, 450–465, https://doi.org/10.1007/s11430-023-1230-3, 2024.

Zheng, B., Tong, D., Li, M., Liu, F., Hong, C., Geng, G., Li, H., Li, X., Peng, L., Qi, J., Yan, L., Zhang, Y., Zhao, H., Zheng, Y., He, K., and Zhang, Q.: Trends in China's anthropogenic emissions since 2010 as the consequence of clean air actions, Atmos. Chem. Phys., 18, 14095–14111, https://doi.org/10.5194/acp-18-14095-2018, 2018.

Supplementary information

Table S1. Correspondence between the seven MCR-CO_2 sectors and EDGAR source category codes, with process definitions and exclusions. Aviation and shipping are companion layers outside the terrestrial-sector sum.

MCR sector	EDGAR monthly 0.10°	EDGAR annual source category codes	Accounting definition and exclusions
POWER	POWER	ENE	Electricity and heat generation (1A1a); exclude categories assigned to fuel transformation and industrial combustion.
INDUSTRY	INDCOM + INDPROC	IND, IRO, NFE, NMM, CHE, NEU, SOLV	Industrial fuel use and matched process CO_2; categories are assigned without double allocation to Power or Fuel.
TRANSPORT	TRANS: aggregate; not land only	ROAD + TNR_OTHER	Terrestrial transport only. The broader EDGAR monthly TRANS aggregate also contains aviation and shipping; these are supplied only as separate companion layers, so the complete total does not count them twice.
BUILDINGS	BLD	RCO	Commercial, institutional and residential stationary activities; mobile transport and industrial process CO_2 remain outside Buildings.
FUEL	FUEL	FOSSIL + REFTRF	Fuel extraction, transformation and refining activities with matched process definitions. Comparisons remain sensitive to power/industry crosswalk boundaries.
AGRICULTURE	AGR	AGS	Included anthropogenic agricultural CO_2 processes only. Agriculture/forestry fuel combustion, liming and urea categories require process-specific matching; vegetation is an allocation proxy, not a CO_2 measurement.
WASTE	WASTE	WASTE_INC	Matched waste-related CO_2 processes, especially incineration. Waste handling of fossil and biogenic CO_2 differs by source; CH_4 and N_2O are outside the MCR CO_2 product.
AVIATION	Included in TRANS	AVI_CDS, AVI_CRS, AVI_LTO, AVI_SPS	Separate aviation companion layer; excluded from the terrestrial inventory sum and included once in the complete inventory.
SHIPPING	Included in TRANS	SHIP	Separate shipping companion layer; excluded from the terrestrial inventory and included once in the complete inventory. Domestic/international geographic attribution follows source coverage.



686

687 Figure S1. Monthly CO_2 emissions for selected locations, illustrating historical changes in the reconstructed emission patterns and the
688 distinction between originally and newly represented emitting cells.

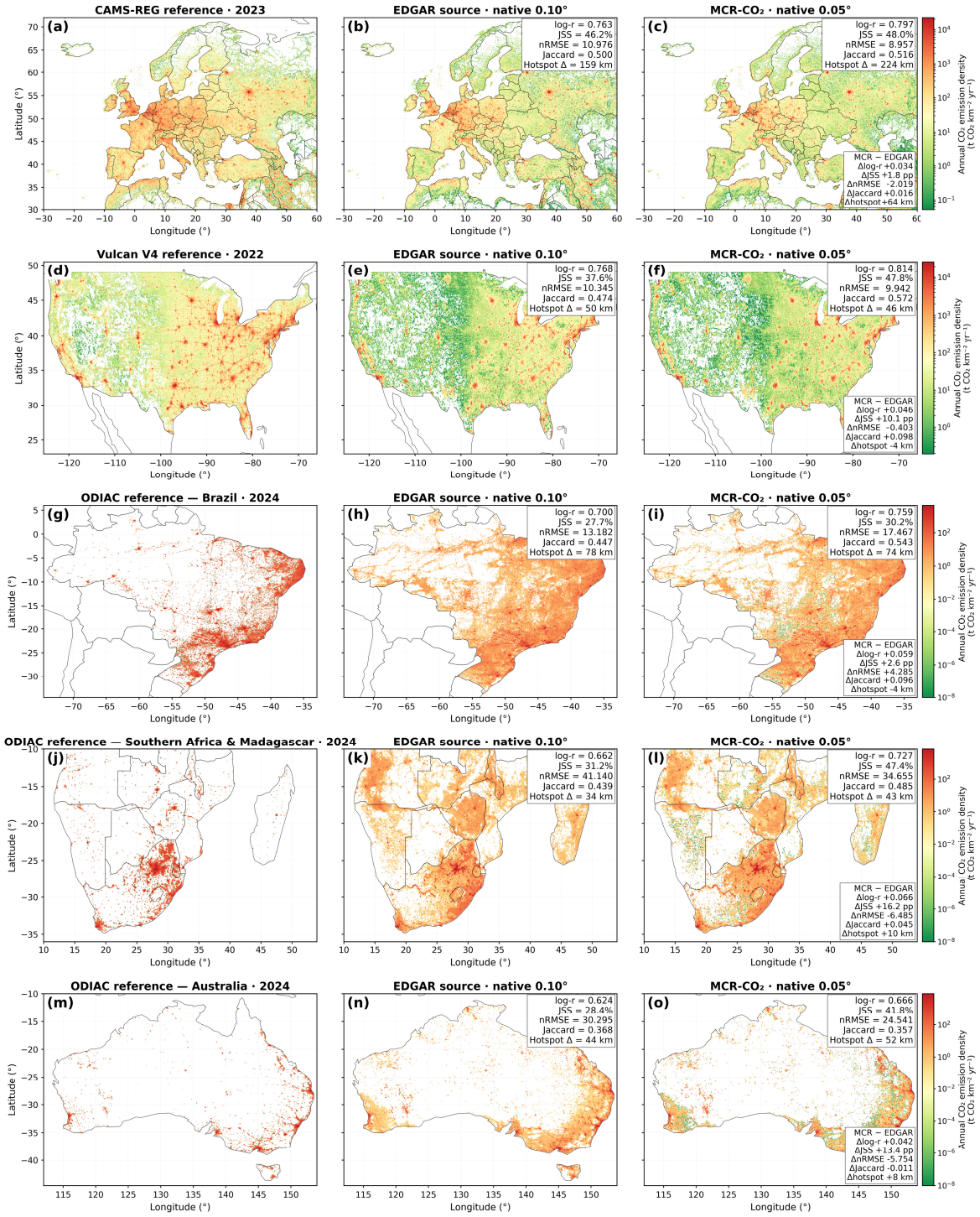


Figure S2. Regional comparison with CAMS-REG, Vulcan V4 and ODIAC in five domains. Rows show the reference, EDGAR at 0.10° and MCR-CO₂ at 0.05° for Europe in 2023 (a–c), the conterminous United States in 2022 (d–f), Brazil in 2024 (g–i), southern Africa and Madagascar in 2024 (j–l), and Australia in 2024 (m–o). Densities are in t CO_2 km^{-2} yr^{-1} on valid reference support. Statistics comprise log-scale correlation, JSS, normalised RMSE, top-decile hotspot Jaccard overlap and centroid displacement. Native-product comparisons include budget and placement differences. ODIAC also contributes to allocation, so its comparisons assess consistency. MCR-CO_2 and EDGAR use the Power, Industry, Buildings and Fuel bundle; reference maps retain their available fossil-emission totals. Sector coverage differences therefore qualify the interpretation of absolute error metrics.

Table S2. Regional comparison of monthly emission profiles on common temporal and geographical support, including Jensen–Shannon similarity, RMSE, normalised error, seasonal correlation and amplitude.

Region	Dataset / period	JSS (%)	RMSE (pp)	nRMSE	r	Amplitude (pp)
Africa	MCR-CO_2 — Pre-2000	99.55 [99.07–99.84]	0.088	0.566	0.898	0.974
Africa	MCR-CO_2 — Post-2000	99.17 [98.69–99.50]	0.167	0.367	0.956	1.006

Region	Dataset / period	JSS (%)	RMSE (pp)	nRMSE	r	Amplitude (pp)
Africa	MCR-CO_2 continuity — 2000 boundary	99.25 [99.20–99.33]	0.149	0.519	0.914	1.209
Africa	MEIC — Pre-2000	99.39 [98.22–99.58]	0.120	0.709	0.740	0.898
Africa	MEIC — Post-2000	96.96 [95.84–97.91]	0.607	1.156	-0.076	0.494
Africa	ODIAC — Post-2000	97.76 [95.16–98.30]	0.443	0.928	0.379	0.425
Africa	EDGAR — Post-2000	99.96 [99.88–99.98]	0.008	0.019	1.000	0.994
Asia	MCR-CO_2 — Pre-2000	98.95 [97.20–99.58]	0.208	0.337	0.982	0.838
Asia	MCR-CO_2 — Post-2000	99.32 [98.92–99.54]	0.137	0.143	0.991	1.024
Asia	MCR-CO_2 continuity — 2000 boundary	99.41 [99.20–99.51]	0.119	0.113	0.995	1.089
Asia	Li et al. (2026) — Pre-2000	96.98 [96.22–99.20]	0.599	1.118	0.934	1.651
Asia	Li et al. (2026) — Post-2000	98.31 [97.16–98.57]	0.332	0.325	0.959	0.844
Asia	MEIC — Pre-2000	98.46 [94.57–98.79]	0.313	0.637	0.822	1.262
Asia	MEIC — Post-2000	95.02 [94.27–96.03]	0.978	0.942	0.341	0.654
Asia	ODIAC — Post-2000	96.08 [94.36–96.82]	0.777	0.791	0.766	0.359
Asia	EDGAR — Post-2000	99.90 [99.79–99.95]	0.019	0.022	1.000	1.014
Europe	MCR-CO_2 — Pre-2000	98.83 [96.51–99.34]	0.237	0.294	0.981	0.912
Europe	MCR-CO_2 — Post-2000	99.03 [98.47–99.43]	0.200	0.151	0.990	1.027
Europe	MCR-CO_2 continuity — 2000 boundary	99.02 [98.55–99.15]	0.192	0.144	0.993	1.041
Europe	Li et al. (2026) — Pre-2000	93.90 [92.87–98.44]	1.198	1.624	0.947	2.484
Europe	Li et al. (2026) — Post-2000	99.01 [97.61–99.34]	0.203	0.141	0.995	1.067
Europe	MEIC — Pre-2000	99.03 [96.61–99.28]	0.196	0.263	0.972	0.902
Europe	MEIC — Post-2000	96.84 [96.08–97.26]	0.612	0.443	0.972	0.612
Europe	ODIAC — Post-2000	95.45 [94.90–96.24]	0.884	0.642	0.916	0.389
Europe	EDGAR — Post-2000	99.95 [99.88–99.98]	0.009	0.007	1.000	0.998
North America	MCR-CO_2 — Pre-2000	99.42 [98.31–99.58]	0.114	0.247	0.981	0.916
North America	MCR-CO_2 — Post-2000	99.63 [99.38–99.80]	0.074	0.112	0.996	1.000
North America	MCR-CO_2 continuity — 2000 boundary	99.19 [99.17–99.26]	0.158	0.219	0.980	0.912
North America	MEIC — Pre-2000	97.45 [95.86–98.20]	0.509	1.125	0.867	1.736
North America	MEIC — Post-2000	96.12 [94.23–96.85]	0.755	1.188	0.343	1.347
North America	ODIAC — Post-2000	98.21 [93.64–98.42]	0.348	0.521	0.891	0.720
North America	EDGAR — Post-2000	99.95 [99.88–99.98]	0.010	0.015	1.000	1.013
South America	MCR-CO_2 — Pre-2000	99.06 [97.95–99.63]	0.187	0.798	0.762	0.554
South America	MCR-CO_2 — Post-2000	99.04 [98.65–99.30]	0.187	0.475	0.916	1.131
South America	MCR-CO_2 continuity — 2000 boundary	98.87 [98.84–98.88]	0.229	0.406	0.920	0.699
South America	Li et al. (2026) — Pre-2000	97.94 [96.05–99.00]	0.408	1.307	0.058	1.047
South America	Li et al. (2026) — Post-2000	96.90 [95.58–97.41]	0.616	1.214	-0.239	0.573
South America	MEIC — Pre-2000	98.76 [96.53–99.32]	0.245	1.014	0.447	0.788
South America	MEIC — Post-2000	97.34 [96.52–97.91]	0.522	1.076	0.065	0.371
South America	ODIAC — Post-2000	97.63 [96.05–98.18]	0.473	0.979	0.433	0.765
South America	EDGAR — Post-2000	99.95 [99.91–99.98]	0.009	0.020	1.000	0.994
Oceania	MCR-CO_2 — Pre-2000	99.36 [99.05–99.77]	0.126	0.734	0.858	1.061

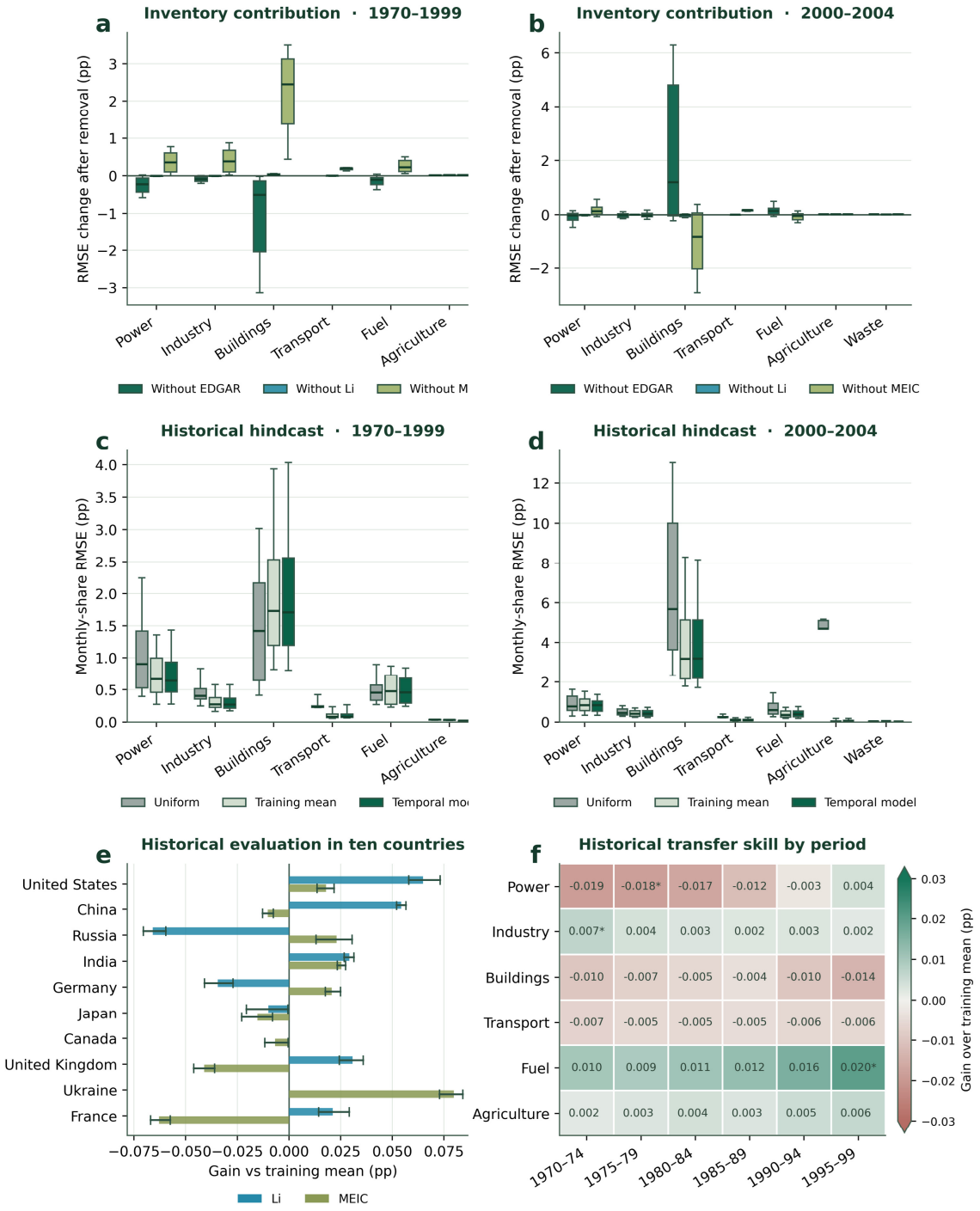


Figure S3. Retrospective evaluation of reconstructed monthly CO_2 emission shares. Panels (a, b) report paired changes in monthly-share RMSE when EDGAR, Li et al. or MEIC is withheld in the stated historical and recent windows; positive differences mean that the retained source reduces error. Panels (c, d) compare monthly-share RMSE against equal one-twelfth allocation and the training-period mean seasonal composition. Panel (e) shows country-level differences relative to that training-mean baseline, and panel (f) summarises successive historical five-year windows.

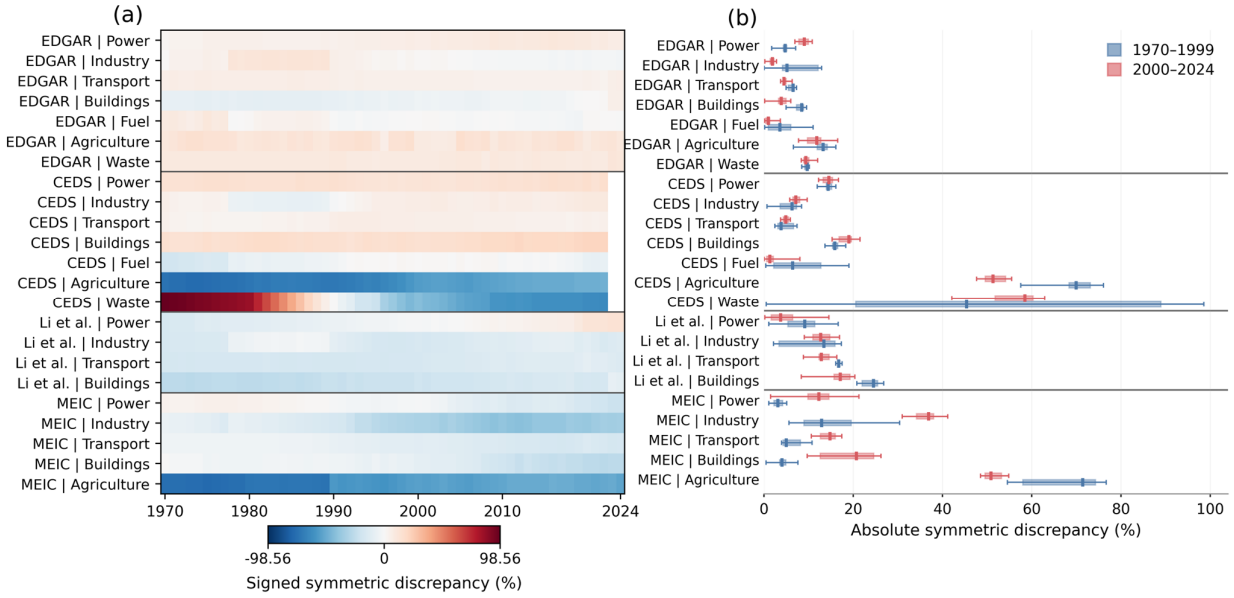


Figure S4. Historical sectoral discrepancies between MCR-CO_2 and compatible EDGAR, CEDS, Li et al. and MEIC estimates over 1970–2024. (a) Annual signed symmetric percentage discrepancies, retaining the direction of each source difference. (b) Absolute symmetric percentage discrepancies for matched source–year comparisons in 1970–1999 and 2000–2024, with displayed medians and spread. Both panels describe disagreement among compatible inventory estimates rather than independent reconstruction error.

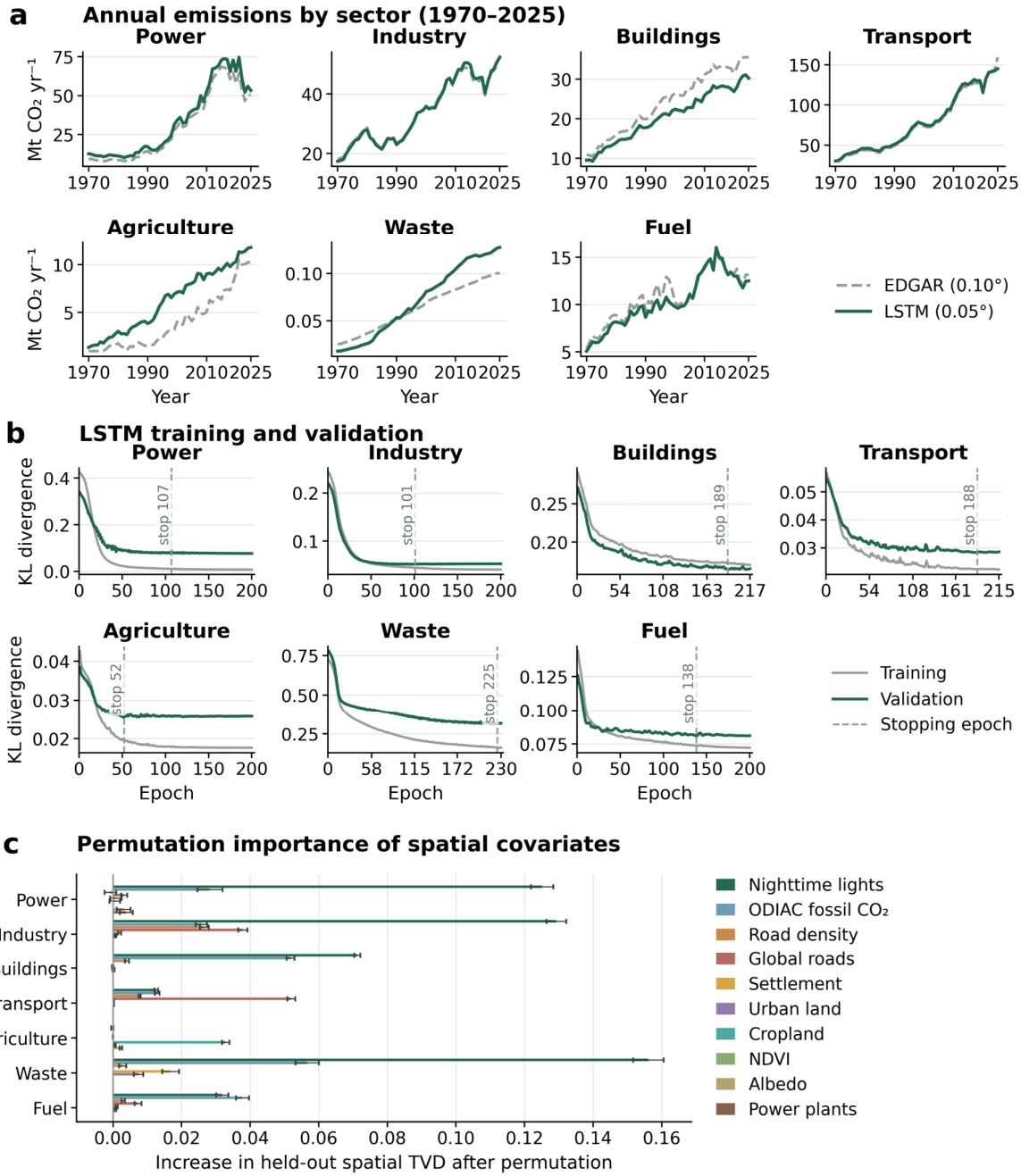


Figure S5. Diagnostics of seven fitted LSTM sector models. (a) Annual sector trajectories in the evaluated region. (b) Training and validation Kullback–Leibler divergence and selected stopping epochs. (c) Held-out predictor permutation importance, measured as the increase in spatial TVD. These diagnostics describe model fitting and predictor dependence. Operational support transfers are restricted to Agriculture and terrestrial Transport under the constraints in Sect. 2.6.

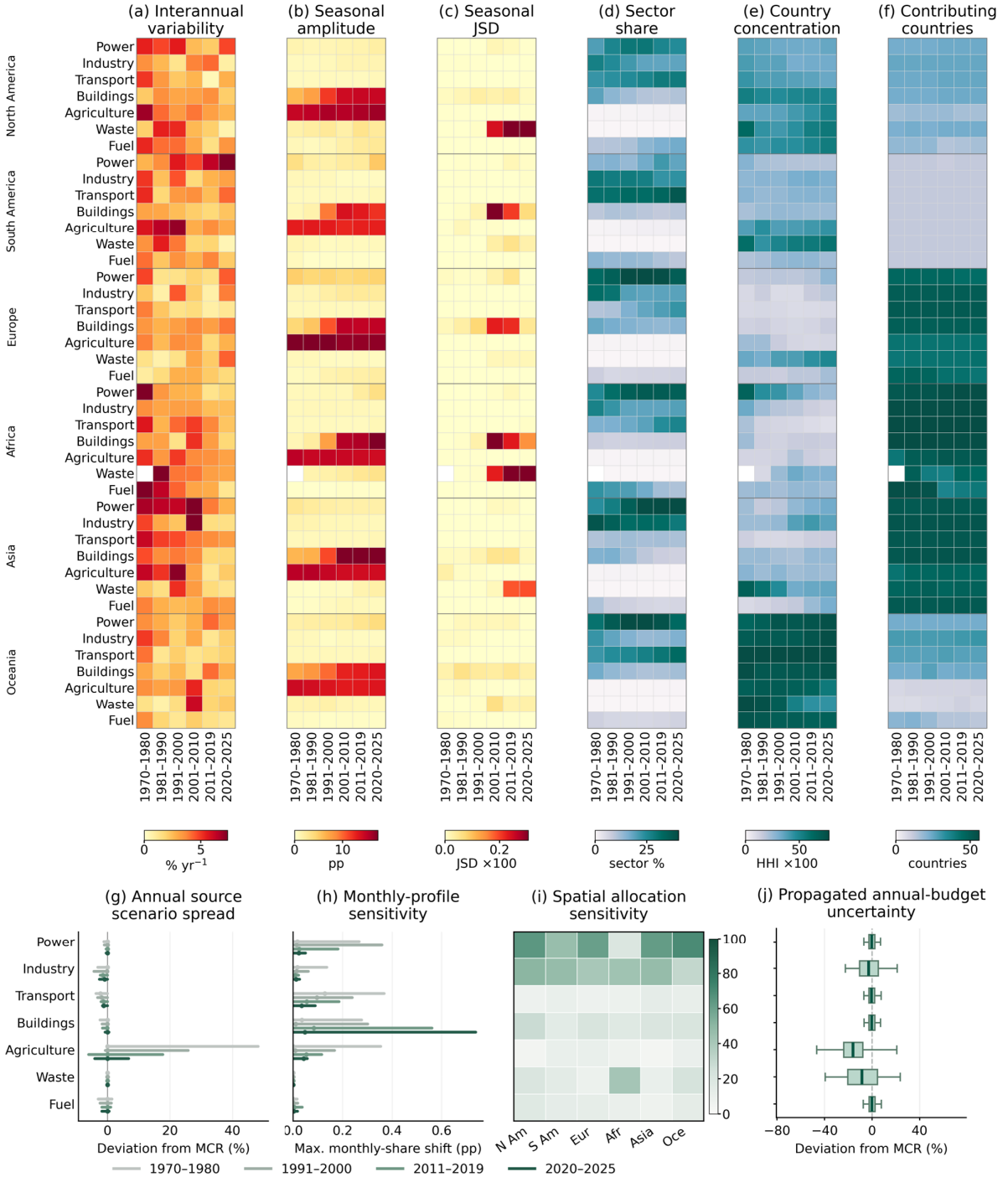


Figure S6. Historical diagnostics, source sensitivity and conditional annual-budget uncertainty. Panels (a–f) show continental and sector medians for 1970–1980, 1981–1990, 1991–2000, 2001–2010, 2011–2019 and 2020–2025. Quantities are (a) absolute annual change (% yr^{-1}), (b) monthly-share amplitude (pp), (c) year-to-year JSD of monthly fractions (×100), (d) sector share (%), (e) country concentration (HHI ×100), and (f) contributing countries. White denotes insufficient temporal support or very low median mass. Panels (g, h) summarise 400 source configurations using annual departures (%) and maximum monthly-share shifts (pp), with medians and outer scenario percentiles. Panel (i) shows TVD (%) for native versus uniform allocation at fixed 0.10° parent mass in June 2024 regional windows. Panel (j) shows 1,000 Monte Carlo annual-budget realisations on country-assigned support over 1970–2025, using transferred Solazzo et al. (2021) CO_2 reference bounds. Boxes span the 25th–75th percentiles, central lines show medians, and whiskers show the 2.5th–97.5th percentiles; the ranges in Tables 5 and S3 are approximate values read from these whiskers. Factors are constant over time and fully correlated across countries within each sector ($\rho = 1$); sectors are sampled independently. Panel (j) conditions on fixed monthly and spatial weights. Tables 4, 5 and S3 distinguish the sensitivity ranges, propagated component and correlation alternatives.

Supplementary methods for annual-budget propagation

The propagation experiment separates uncertain magnitude from normalised allocation. Write a country–sector grid-cell emission as its annual budget multiplied by a monthly fraction and a final spatial fraction. With both fractions fixed,

multiplying the annual budget by F multiplies every associated cell and every within-country transfer by F. Relative variance is therefore inherited directly, while conservation holds for each realisation. The result applies to the annual-budget component on the assigned country masks.

Country correlation is imposed in log-factor space. A common sector draw and a country–sector draw are combined using square-root weights, as shown in Eq. (19). The main $\rho = 1$ case avoids reducing a shared sector uncertainty merely by summing many countries. The $\rho = 0$ and 0.5 cases quantify sensitivity to alternative cross-country dependence; their aggregate full-record intervals are reported in Table S3.

Bounds are transferred from global 2015 IPCC categories to MCR-CO_2 sectors and years. They are a reference parameterisation, not country-specific EDGAR uncertainty estimates. Industry combines combustion and industrial processes, so an additional Energy-only reference of ±7.1% was evaluated. This alternative gives a central 95% Industry interval of −7.33% to +7.25%, compared with approximately −23% to +21% using IPPU (Fig. S6j).

Under the main model, every country within a sector shares the same distributional parameters and the same factor in each realisation. Relative sector intervals are consequently identical across the six reporting periods, regardless of their emission weights. Under partial or independent country errors, aggregation depends on country shares. The annual table contains 91,336 country–sector–year rows, with input checks rejecting duplicate records, non-finite values and negative totals. Zero-emission combinations remain zero.

Table S3 intervals concern the full 1970–2025 country-assigned record. They exclude uncertainty in monthly composition, geographical location, sector definitions, support selection and mass outside the assigned country masks. Source-choice and predictor-removal diagnostics report complementary sensitivities without converting them into independent probability distributions.

Table S3. Sensitivity of central 95% annual-budget Monte Carlo intervals to cross-country error correlation. Values are percentage departures for aggregated 1970–2025 country-assigned sector emissions. Each case uses 1,000 realisations and the same transferred bounds. ρ denotes correlation of the Gaussian log factors within a sector; different sectors are sampled independently.

Sector	**ρ = 0 (%)**	**ρ = 0.5 (%)**	**ρ = 1 (%)**
Power	−2.46 to +2.12	−5.44 to +5.19	−7 to +7
Industry	−9.27 to +6.23	−17.47 to +15.49	−23 to +21
Transport	−2.52 to +2.31	−5.23 to +5.57	−7 to +8
Buildings	−2.25 to +1.79	−5.09 to +4.84	−7 to +7
Agriculture	−40.90 to +1.71	−64.28 to +41.18	−47 to +21
Waste	−19.96 to +10.00	−31.45 to +26.48	−39 to +24
Fuel	−1.98 to +1.75	−5.64 to +5.68	−7 to +8